

Channel Sounding for D-Band Measurements

Samantha M. Frietchen

Thesis submitted to the Faculty of the
Virginia Polytechnic Institute and State University
in partial fulfillment of the requirements for the degree of

Master of Science
in
Electrical Engineering

Alan J. Michaels, Chair
Harpreet S. Dhillon
Carl B. Dietrich

February 11th, 2025
Blacksburg, Virginia

Keywords: Channel Sounding Techniques, SDR, D-Band, Sub-Terahertz Communication,
Path Loss

Copyright 2025, Samantha M. Frietchen

Channel Sounding for D-Band Measurements

Samantha M. Frietchen

(ABSTRACT)

With the advent of new technologies introduced with each cellular generation, there is need to characterize a variety of different communications links. Areas, such as software defined radios, have been explored to fill flexibility needs for dynamic sounding. Also of heavy interest is exploring the terahertz frequency band for communication potential in 6G. However, numerous channel sounding measurements must be collected to properly support channel models for this region. The work detailed in this thesis aims to address this current research areas, with three main contributions: (1) detailing a flexible software define radio channel sounding architecture for easy, configurable channel sounding, (2) a comparison of sounding waveforms within a software defined radio framework, and (3) a detailed D-Band channel sounding framework and short-range path loss measurements. In the first contribution, a low cost radio (Ettus B210) is used as the channel sounding transmitter with a frequency retuning software to overcome the small instantaneous bandwidth of the low cost transmitter. In the second contribution, an upgraded version of the SDR channel sounder transmitter from the first contribution is used to compare different sounding waveforms. Each of the waveforms were tested within the same channel sounder architecture and the results were compared to make recommendations about which waveform to use in a variety of circumstance. In the third contribution, a new channel sounder, with sub-THz up and down conversion, was used to collect path loss measurements at D-Band. In these contributions, we target addressing two prominent areas of channel sounding research: use of low-cost radios for channel sounding and (sub-)terahertz frequency channel characterization.

Channel Sounding for D-Band Measurements

Samantha M. Frietchen

(GENERAL AUDIENCE ABSTRACT)

In communications, sending information is done by modulating information bits in a signal that can be sent from the sender to the receiver. The environment, or channel, in between the sender and receiver plays a significant role in whether the information is successfully received. Thus, in developing of communications links, it is important to have an understanding of how the channel behaves and affects the information signal. Channel sounding is a process of collecting measurements that characterize the behavior of the channel. In recent years, more devices are being connected, creating new environments to be characterized, which require flexibility in channel sounder design. Additionally, with new devices, there is interest in leveraging higher portions of the RF spectrum. Moving up in frequency introduces new challenges in successfully communicating, but higher frequencies offer the reward of accessing greater bandwidth and thereby data throughput. In this work, we (1) detail the design of a channel sounder using low-cost hardware, (2) analyze the performance achieved using different waveforms for sounding on low-cost hardware, and (3) collect measurements using a live hardware system capable of measuring at high frequencies, 120-130 GHz.

Dedication

To my mom, my first teacher

Acknowledgments

There are several individuals I would like to thank for their support in making my research possible, whether that be through guidance, assistance, or moral support. First, I have been extremely fortunate to work with Andres Peñafiel, Cameron Williams, Olivia Watt, Jake Frohlic, and Andrew Brown, all of whom are talented undergraduate students. These students have assisted me in various meaningful capacities ranging from measurement collection, GUI design, to embedded programming.

I would also like to extend a huge thank you to the members of my research team who have all been a pleasure to work with: Michael Fletcher, Dr. Brad Davis, Dr. Daniel Jakubisin, and Dr. Alan Michaels. Michael Fletcher's work in designing and assembling the the sub-THz hardware system has been instrumental in my research. He also would often leave his door open and be very accessible to talk to and ask questions. Dr. Davis has always been extremely helpful and insightful to speak with, even despite working on a separate part of the project as me. I really appreciate the effort that Dr. Jakubisin has put into reading over my paper drafts as well as taking time to work through various technical challenges I have faced throughout my graduate school journey. He is an excellent listener and his advice is always well-thought out and in line with scope of the project. My advisor, Dr. Michaels, is an individual who cares deeply about his students and propping them up to succeed. He is not afraid to give students a degree of independence when solving challenging, meaningful problems, and offers genuine guidance and feedback in an extremely timely manner (most paper edits back within 24 hours!). Overall, I've been privileged to work with and learn from an amazing group of people. I also want to recognize my committee members, Dr. Dhillon and Dr. Dietrich, for being excellent professors and taking the time to hear about

my research.

The last group of people that deserves recognition and my deepest thanks is my support system. Fellow graduate students, Sam Brown, Emily Tirrell, Will Poland, and Hannaneh Shadabi, have been refreshing to connect to and inspiring to look up towards. Despite the new distance, my undergraduate friends, Esther Palmer, Sara Larson, Isabel Hasson, and Gillian Murphy, have managed to keep me sane even in times of stress. Last, but certainly not least, I would like to thank my family, my sister, Rachel Andrade-Frietchen, my mom, Kelly Frietchen, my dad, Douglas Frietchen, and my partner, Siraj Syed, for their endless support and providing motivation for me to make them proud.

Contents

List of Figures	xi
List of Tables	xiv
1 Introduction	1
1.1 Motivation	1
1.2 Contributions	4
2 Review of Literature	7
2.1 Propagation through the Wireless Channel	7
2.1.1 Large-Scale and Small-Scale Fading	7
2.1.2 Channel Impulse Response	9
2.1.3 Power Delay Profile	11
2.2 Channel Measurement Collections	13
2.2.1 Direct Pulse	13
2.2.2 Vector Network Analyzer (Frequency Domain)	13
2.2.3 Pulse Compression	14
2.3 Channel Sounding Applications	14

3	Channel Sounding Transmitter Design with Software Defined Radios	16
3.1	Abstract	16
3.2	Motivation	17
3.3	Experimental Framework	19
3.4	Design and Implementation	20
3.4.1	Control Features and the User Interface	21
3.4.2	Baseband FMCW Waveform Generation	23
3.4.3	Transmitter Manager and Retuning	24
3.5	Initial Validation	26
3.5.1	End-to-End Transmission Demonstration	26
3.5.2	Quantifying Dwell Time	28
3.6	Conclusions and Future Work	29
4	Waveform Selection Comparison	31
4.1	Abstract	31
4.2	Motivation	32
4.3	Baseband Waveform Selection and Comparison	36
4.3.1	Channel Sounding Waveforms	37
4.3.2	Processing Techniques	41
4.3.3	Channel Estimation Technique Performance	43

4.4	Experimental Setup	46
4.4.1	Low-Cost Hardware Considerations	50
4.5	Over-the-Air Measurements and Discussion	52
4.5.1	Performance Analysis / Scenarios	55
4.6	Conclusions and Future Work	57
5	D-Band Path Loss Measurements	62
5.1	Abstract	62
5.2	Motivation	63
5.3	Wideband Channel Sounding System Architecture	67
5.3.1	Hardware Architecture: RF Front End	67
5.3.2	Channel Sounding Packet Structure	69
5.3.3	Transmission Manager	72
5.3.4	FPGA Mechanics	75
5.3.5	Receiver Post Processing	76
5.4	Preliminary Measurement Collection	79
5.4.1	Experimental Setup	79
5.4.2	Link Budget of System	79
5.4.3	Short Range Path Loss Measurements	80
5.5	Conclusions and Future Work	84

6	Conclusions	86
6.1	Discussion	86
6.2	Recommendations for Future Work	90
	Bibliography	93

List of Figures

1.1	Flow from channel measurements to systems implementation	2
1.2	Flow from channel measurements to systems implementation	4
2.1	Visualization of small-scale and large-scale fading	8
2.2	Graphics illustrating various propagation phenomena	10
2.3	Visualization of a communication scenario and the resulting PDP	12
3.1	Illustration of Achieving Approximate Desired Wideband Channel Sounding Signal with Intermediate Transmissions	20
3.2	Block diagram showing the experimental setup of wideband channel sounding	21
3.3	Control interface to configure the wideband transmission	22
3.4	Diagram to show center frequency adjustment algorithm in TX manager . .	25
3.5	IQ Recorder waterfall plot to show end of 1 GHz frequency sweep n (right hand) and the start of sweep n+1 (left hand)	27
3.6	IQ Recorder waterfall plot and persistence plot to show 80 MHz down sweep	27
4.1	Visualization of Discrete Time-Varying Channel	37
4.2	Time and Frequency Domain Representations for Channel Sounding Waveforms	38
4.3	Instantaneous Power Distributions for Five Repetitions of Each Sounding Waveform with Power Fade in Filter Applied	45

4.4	Channel Sounding Transceiver Block Diagram	46
4.5	Baseband Received Spectrogram showing Channel Sounding Blocks at Various Center Frequencies	47
4.6	Post Processing Algorithm by Waveform Block Diagram	49
4.7	Envelope of USRP RF Front End Filter Transient Response with Each of the Waveforms	51
4.8	Visuals of Environment used to Collect Measurements with Metal Bin Reflectors	52
4.9	Envelope of Power Delay Profile with Each of the Sounding Waveforms	53
4.10	Power Delay Profile Obtained from FMCW and PN Stimulus Highlighting Sharp PN Decay	54
4.11	Waveform Channel Sounding Performance based on Specific Sounding Metrics - Spider Diagram	58
4.12	Waveform Channel Sounding Performance based on Specific Sounding Metrics - Multi-Category Bar Diagram	59
5.1	Full System Architecture	68
5.2	Frame ID Structure	69
5.3	TX Manager Block Diagram	73
5.4	TX manager communications between host machine, frequency synthesizer, and FPGA	74
5.5	Two received packets correlated with transmitted pulse to illustrate time alignment for packet decomposition and analysis	77

5.6	Hardware Setup	78
5.7	Received signal strength across D-Band frequencies and short range distances	81
5.8	Received signal strength across D-Band frequencies and short range distances relative to waveguide measurements	82
5.9	Path loss measurements from 120 - 130 GHz normalized to waveguide mea- surements	83

List of Tables

3.1	Control features for the wideband transmission, their description and possible input values	23
3.2	Parameters for the TX Manager Effecting the Transmission	26
3.3	Transmission settings corresponding to the frequency sweep shown in Fig. 3.5.	27
3.4	Transmission settings corresponding to the frequency sweep shown in Fig. 3.6.	28
3.5	Dwell time measurements	29
4.1	Waveform Configuration Parameters that Inform Signal Generation	39
4.2	Instantaneous Power Distribution Statistics	45
4.3	Summary of the Strengths, Challenges and Recommended Scenarios for each of the Sounding Waveforms Explored	60
5.1	Link Budget of Example -13.2 dBm Sinusoidal	79

List of Abbreviations

ADC Analog to Digital Converter

BW Bandwidth

CAZAC Constant Amplitude Zero Autocorrelation

CDF Cumulative Distribution Function

CF Center Frequency

CI Close-In

CIR Channel Impulse Response

CRC Cyclic Redundancy Check

CSI Channel State Information

CW Continuous Wave

DAC Digital to Analog Converter

DSA Dynamic Spectrum Access

DUT Device Under Test

FFT Fast Fourier Transform

FI Floating Intercept

FMCW Frequency-Modulated Continuous Wave

FPGA Field Programmable Gate Array

FSK Frequency Shift Keying

GUI Graphical User Interface

IF Intermediate Frequency

IFFT Inverse Fast Fourier Transform

IQ In-Phase and Quadrature

LNA Low Noise Amplifier

mMIMO massive-MIMO

mmW Millimeter Wave

MPC Multipath Component

NCO Numerically Controlled Oscillator

OFDM Orthogonal Frequency-Division Multiplexing

OOT Out of Tree

PAPR Peak-to-Average Power Ratio

PHY Physical

PN Pseudo-Random Noise

RF Radio Frequency

ROM Read-Only Memory

RX Receive

SDR Software Defined Radio

SRA Scheduling and Resource Allocation

STDCC Swept-Time Direct Cross Correlation

sub-THz sub-Terahertz

THz-TDC Terahertz Time Domain Correlation

THz-TDS Terahertz Time Domain Spectroscopy

TX Transmit

UART Universal Asynchronous Receiver / Transmitter

UHD Universal Software Radio Peripheral Hardware Driver

USRP Universal Software Radio Peripheral

V2V Vehicle-to-Vehicle

VCO Voltage Controlled Oscillator

VNA Vector Network Analyzer

Chapter 1

Introduction

1.1 Motivation

An understanding of how the wireless channel interacts with a emitted signal is crucial for successful deployment of a communication system. Channel sounding is the technique of collecting measurements that aim to characterize the wireless channel, particularly in different environments and at different frequency ranges. Fig. 1.1 shows the general progression or pipeline that leads from channel measurements to actual system deployment. One caveat is that this progression does not show dynamic adjustments to system constraints made after deployment. Thus, the driving motivation behind collecting channel measurements is to gauge limitations of operating within a specific environment or frequency range, ultimately constructing predictive models, so that system deployment is successful. An excellent case study in the relationship channel sounding has on communication system infrastructure is from Rappaport's group on mmWave for 5G communications [62]. In this work, measurements made within an urban environment inform recommendations of base station separation. Sounding campaigns can aim to characterize a variety of phenomena associated with the channel that need to be accommodated for in a communication system, such as, path loss, delay spread, angle of arrival, and Doppler spread. Thus, channel sounding covers a wide breadth of environments and scenarios to characterize, from diffraction off a person [55] to real-time, directional vehicle-to-vehicle (V2V) characterization [15]. Each specific

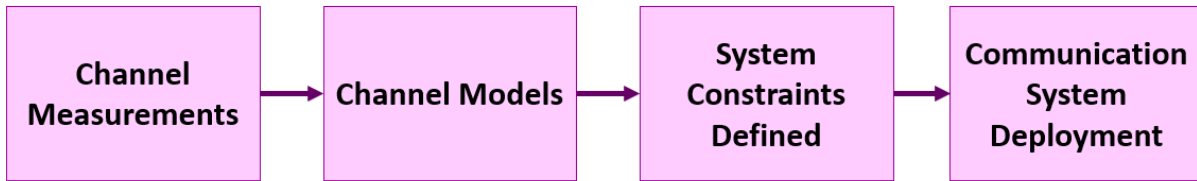


Figure 1.1: Flow from channel measurements to systems implementation

measurement campaign has different requirements needed from the channel sounder based on assumptions from the channel behavior and what is targeted to measure.

Software Defined Radios (SDRs) have been explored heavily in their applicability to channel sounding. While imposing some limitations, namely low instantaneous bandwidth, dynamic range, and accessible frequency range [79], SDRs are significantly more accessible and flexible compared to more custom architectures [65]. Operating within Dynamic Spectrum Access (DSA) environments, a spectrum efficiency technique allowing a secondary user to select unused bands to transmit over, is a specific case where the flexibility of SDRs is appealing. In [12], a channel sounder is used as a secondary user and requires the channel sounding to dynamically adjust power based on the primary users presence within the band.

With channel sounding being such a broad field, there are several scenarios that aim to measure different phenomenon of the channel. For example, in [55], an analog sliding correlator was used for coverage analysis because this architecture compresses the receive bandwidth and eases ADC sampling rate requirements. However, this architecture sacrifices Doppler resolution and thus a different hardware architecture was used for measuring the Doppler spectrum. While this example specifically illustrates the impact of hardware architecture on various performance metrics, the selection of sounding waveform and post processing technique also plays a role on performance constraints. Common waveforms that are used to stimulate the channel include frequency-modulated continuous wave (FMCW), binary

pseudo-random noise (PN), Orthogonal Frequency-Division Multiplexing (OFDM), Zadoff-Chu, and Direct Pulse. There exists some comparisons of the waveforms [52], [71], [72], but these comparisons do not offer contextualization for different channel sounding scenarios.

Emergence of new, data-rate intensive technologies, like holographic communications and extended reality applications, motivates exploring potential use of the terahertz (THz) band (0.1-10 THz) for communications [75]. As mentioned previously and illustrated by 1.1, an important first step is characterizing the channel environment. One band of interest for communications within the THz band is D-Band ranging from 110 to 170 GHz [4]. D-Band measurement campaigns have been conducted to measure path loss [68], penetration losses [44], and foliage losses [75], to name a few. Despite these campaigns, sub-THz channel measurements remains an active area of research because a large body of measurements from different organizations is required for accurate statistical models [4].

The work presented in this thesis aims to address some of these active research areas in channel sounding. Fig. 1.2 shows the high level operational concept graphic of the sounding architectures described in this thesis. Note that different sounding architectures are detailed, a low-cost frequency-limited SDR based channel sounder and a custom FPGA-based hardware D-Band channel sounder. Through the following chapters of this thesis the following contributions will be addressed:

- Design of a flexible, low-cost channel sounding transmitter with the ability to aggregate intermediate transmissions to achieve a larger bandwidth across any frequency range within the operational constraints of the SDR.
- Comparison of sounding performance when using FMCW, Zadoff-Chu, OFDM, PN, and direct pulse waveforms on an SDR using qualitative analysis of performance metrics and observation of over the air performance.

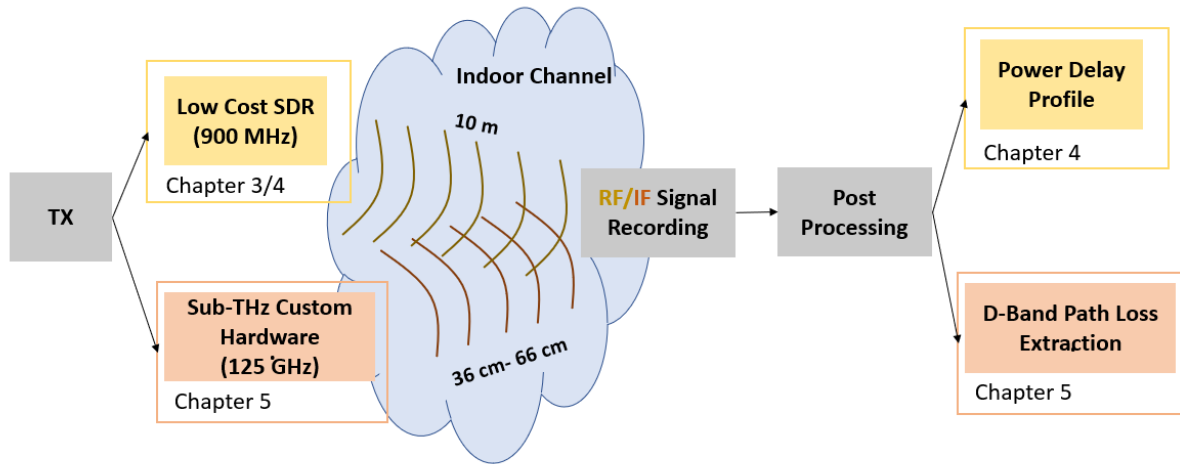


Figure 1.2: Flow from channel measurements to systems implementation

- Details on a flexible D-Band channel sounder capable of selecting sounding waveforms, bandwidths, and measured frequency ranges. The realized system used to collect short-range path loss measurements with Zadoff-Chu stimulus.

1.2 Contributions

The work detailed in this thesis pertains to practical implementations for channel sounding research that are tailored towards emerging channel sounding applications. The main body chapters are supported with hardware development on various platforms, including software defined radios, digital signal recorders, and D-Band hardware conditioning. Chapter 2 details relevant background knowledge regarding propagation mechanics, measurement systems, and current channel sounding directions applicable to this work.

Chapter 3 details the design of a flexible, low-cost channel sounding transmitter that is implemented on an Ettus USRP B210. The channel sounder uses a frequency-modulated

continuous wave signal to stimulate the channel and is equipped with retuning software to obtain a larger bandwidth than the relatively narrow instantaneous bandwidth of the B210. The channel sounder has the ability of making flexible selections of start frequency, full transmission bandwidth, and sweep duration. This chapter is adapted from the below publication cited as [28].

- Samantha Frietchen, Daniel J. Jakubisin, and Alan J. Michaels. Semi-Automation of Wideband Channel Sounding Transmitter. In 2024 IEEE International Symposium on Dynamic Spectrum Access Networks (DySPAN), pages 145–150, 2024. doi: 10.1109/DySPAN60163.2024.10632753.

Chapter 4 performs a comparison of the channel sounding performance using different waveforms within the context of a software defined radio. A flexible channel sounding architecture was detailed, modified from the version listed in Chapter 3, that allows for dynamic selection of channel sounding waveform. With this setup, an indoor channel was measured using a direct pulse, Zadoff-Chu, FMCW, OFDM, and PN sequence for comparison. This chapter is adapted from the below publication cited as [30].

- Samantha Frietchen, Daniel J. Jakubisin, and Alan J. Michaels. Channel Sounding Waveform Comparison using Software Defined Radios. In 2025 the 5th European Conference on Communication Systems (ECCS 2025), 2025. [Accepted].

Chapter 5 contains path loss measurements collected at D-Band from a short range in a laboratory setting. The full channel sounding setup is detailed, including hardware architecture for D-Band up and down conversion, transmission coordination, channel sounding packet structure, FPGA mechanics as an IF source, and post processing software for path loss extraction. The architecture is capable of measuring the channel across D-Band, but

this chapter focuses on the range 120-130 GHz. Due to constraints on the current hardware architecture setup, the distance capable of being measured was limited to less than 0.5m. Thus, measurements were collected across 120-130 GHz at distances of 36 cm, 45 cm, and 66 cm. This chapter is adapted from the below publication cited as [29].

- Samantha Frietchen, Michael J. Fletcher Daniel J. Jakubisin, and Alan J. Michaels. D-Band Path Loss Measurements and Frequency Stability Characterization. In 2025 the 5th European Conference on Communication Systems (ECCS 2025), 2025. [Accepted].

Chapter 6 consolidates the findings made throughout each of the previous chapters to make overall conclusions. Also detailed within this chapter are recommendations for future work based upon the current findings from this thesis.

Chapter 2

Review of Literature

2.1 Propagation through the Wireless Channel

Communication requires transport of a signal encoded with information through some kind of medium from one point to another. Oftentimes, the characteristics of the transport medium affect the ability for the desired signal to successfully reach the intended receiver. In wireless communications, obstacles present within the physical environment between emitters interact with radiated signals leading to consequences within the received signal. Thus, it is important to develop an understanding of the wireless channel to ensure successful communications.

2.1.1 Large-Scale and Small-Scale Fading

Fading is degradation in signal strength from interactions with the channel and can be categorized into large-scale or small-scale fading [61]. Large-scale fading represents trends in signal strength that are steady across distance. The main phenomena that contribute to large-scale fading are path loss and shadowing [47]. Path loss encompasses the average decrease in signal strength observed by the receiver as distance between transmitter and receiver increases. Free space path loss is defined by Eqn 2.1.1 and is influenced by transmit power (P_t), transmit antenna gain (G_t), receive antenna gain (G_r), signal wavelength (λ), and distance between TX and RX (d) [61]. Shadowing is the result of a major physical

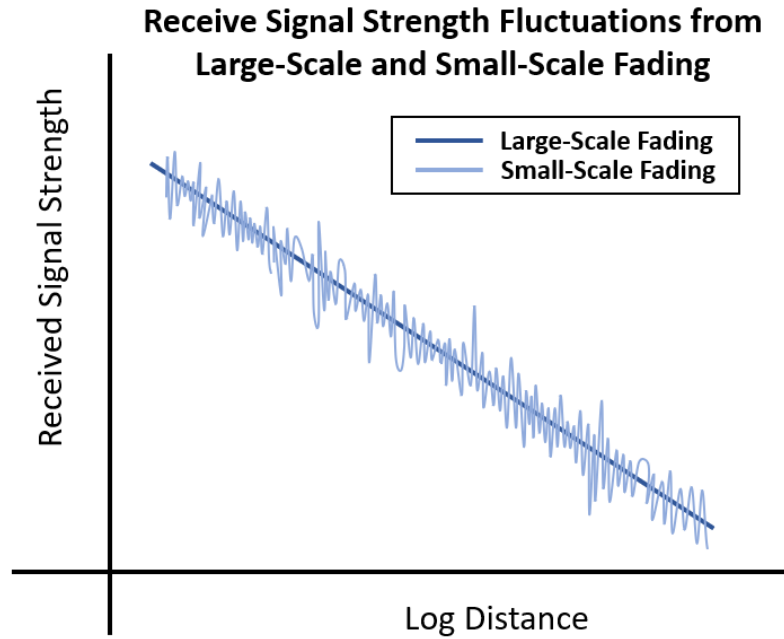


Figure 2.1: Visualization of small-scale and large-scale fading

object, such as a mountain, that obstructs the signal's path, resulting in deviations in signal strength consistent across a relatively large distance.

$$FSPL = \frac{G_t G_r \lambda^2}{(4\pi)^2 d^2} \quad (2.1)$$

Small-scale fading represents how minor differences in placement (in space) and time can result in fluctuations in signal strength. There are often several paths between the transmitter and receiver, due to phenomena such as reflection, diffraction, and scattering [61]. Reflection occurs when a wave meets an object with dimensions much larger than the wavelength of the signal. Shown in Fig. 2.2a, a reflection will redirect the RF signal to a new angle depending upon the reflection coefficient of the material. Diffraction occurs when the RF signal encounters a sharp edge from a surface and the signal energy will be redirected

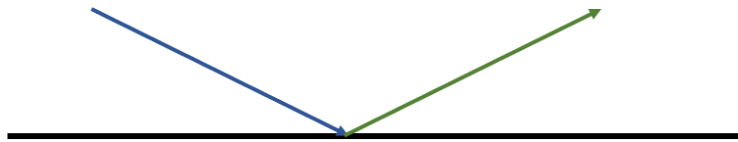
as shown in Fig. 2.2b. Scattering occurs when the signal wavelength is comparable to the surface roughness of the object being met. Observe from Fig. 2.2c, scattering results in several new signal paths with weakened signal strength. The non-Line of Sight (LOS) paths reaching the receiver are termed multi-path components (MPCs) and can lead to signal degradation. Small variations in distance adjustments can lead to drastic changes in signal strength depending upon how the MPCs constructively or destructively interfere with each other.

2.1.2 Channel Impulse Response

The wireless channel may be treated as a time varying linear filter [8], relating TX and RX signals by Eqn. 2.1.2 with the addition of noise. In Eqn. 2.1.2, $x(t)$ is the transmitted signal, $y(t)$ is the received signal, and $h(t,\tau)$ is the time-varying channel impulse response. This representation follows the assumption that the channel is wide-sense stationary with uncorrelated scatters, or behaves wide-sense stationary over a period of time and frequency that is significantly larger than the time and frequencies of interest. With uncorrelated scatters, the received signal can be represented as a summation of time-shifted, phase-shifted and frequency shifted replicas (or echos) of the original transmitted signal. It is beneficial to quantize the delay axis into discrete excess delay bins for the arrival of multipath components [61]. The equation for the complex channel impulse response for a multipath channel (with quantized delay bins) is detailed in 2.1.2.

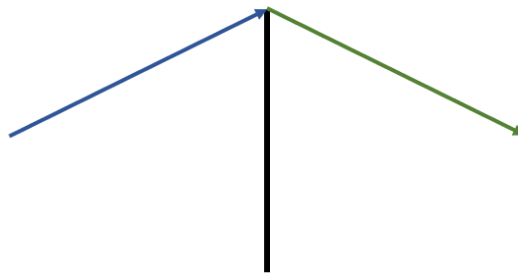
$$y(t) = h(t, \tau) * x(t) + n(t) \quad (2.2)$$

Reflection



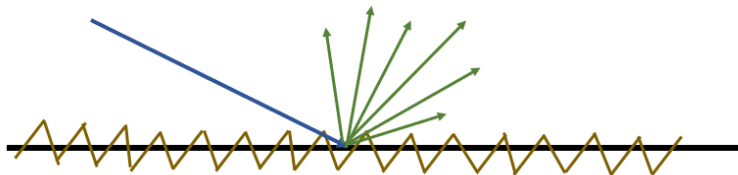
(a) Illustration of reflection

Diffraction



(b) Illustration of diffraction

Scattering



(c) Illustration of scattering

Figure 2.2: Graphics illustrating various propagation phenomena

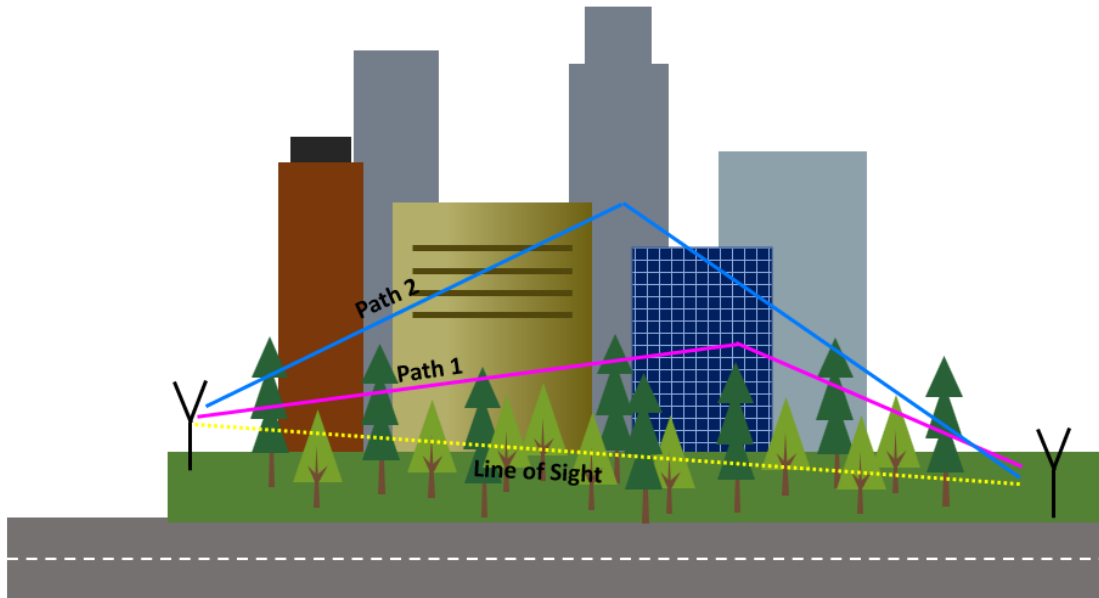
$$h(\tau, t) = \sum_{k=1}^N \alpha_k(t) e^{j\phi_k(t)} \delta(\tau - \tau_k(t)), \quad (2.3)$$

2.1.3 Power Delay Profile

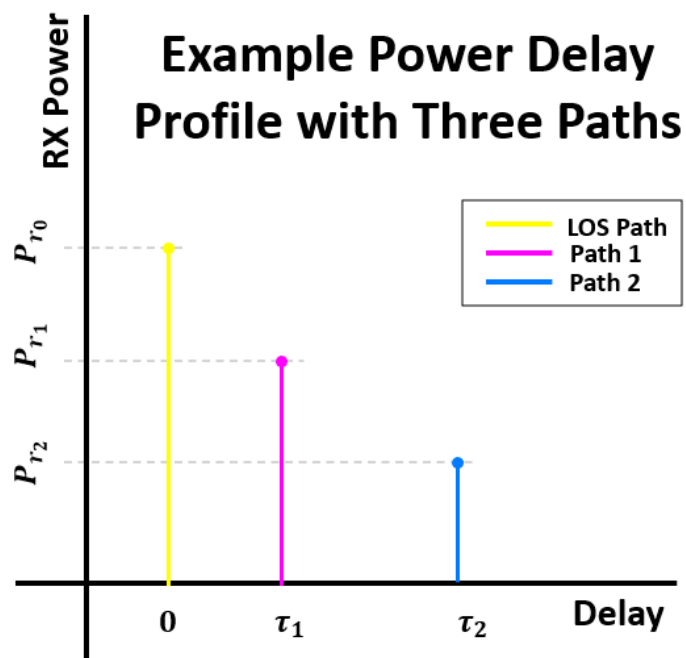
The Power Delay Profile (PDP) characterizes the power at a given delay bin and is calculated by normalizing the time dependence from the CIR. Eqn. 2.1.3 shows how to obtain the PDP from the time varying channel impulse response [42].

$$p_d(t) = \frac{1}{K} \sum_{k=1}^K |h(t_k, \tau)|^2 \quad (2.4)$$

Fig. 2.3. shows an example of a communication link that would result in multipath components affecting the received signal. In Fig. 2.3a, a transmitter and receiver are set up within an urban environment with building obstructions between the emitters. Communications within this environment results in multiple paths between the transmitter and receiver with each path corresponding to a specific time delay and power. Fig. 2.3b is the power delay profile corresponding to this scenario representing the received power strengths at specific delays. Speaking generally, an increase in path length will result in a increased time delay and a decrease in signal strength as illustrated in this example.



(a) Communication within a city landscape with several paths between TX and RX



(b) Corresponding PDP of city landscape communication

Figure 2.3: Visualization of a communication scenario and the resulting PDP

2.2 Channel Measurement Collections

In order to characterize the wireless channel, measurements must be collected with a process called channel sounding. Channel sounding involves simulating the channel through various means and observing the response at the receiver. In the following section, three common channel sounding approaches will be outlined with details on approach as well as strengths and weaknesses.

2.2.1 Direct Pulse

The (periodic) direct pulse method involves observing the channel when stimulated a pulse that resembles the Dirac Delta function. In this approach, the CIR snapshot can be directly observed from synchronization with the received signal. In THz channel sounding this method is termed THz Time Domain Spectroscopy (THz-TDS), typically achieved by using a femtosecond laser for emitting the short duration pulse. In several campaigns, THz-TDS is used to characterize THz propagation phenomena like atmospheric effects and scattering [54, 59].

2.2.2 Vector Network Analyzer (Frequency Domain)

The frequency response of the channel is directly observed in the vector network analyzer (VNA) method of channel sounding [61]. In this approach, a VNA is used with the wireless channel as the device under test (DUT). The VNA will stimulate the channel by stepping through specific carrier frequencies over the desired range and recording the magnitude and phase offsets. From these measurements, the frequency response of the channel is noted by aggregating the response from these discrete carrier steps. Some limitations of these

systems include requiring a direct connection between transmitter and receiver, thus limiting distance, and often require significant time for measurement collection. With use of frequency extenders, the VNA approach can be used to characterize the sub-THz channel [14, 84].

2.2.3 Pulse Compression

Another channel sounding approach involves transmitting a pulse that has an autocorrelation function that approximates the Dirac Delta function. Any multipath components present in the received signal can be extracted from correlation with the transmitted signal. The CIR is estimated by taking the cross correlation between the received signal and the transmitted pulse. This channel sounding approach can require more complex synchronization methods, but can measure the farthest distances compared to the other two approaches [31]. One campaign using the pulse compressed method was able to achieve a TX-RX separation of 117.4 m at 142 GHz sounding frequency [82].

2.3 Channel Sounding Applications

The fifth cellular generation has introduced sidelink communications, allowing for devices to directly communicate with each other [58]. Sidelink communication is useful in the context of Internet of Things (IoT), allowing for sensors and embedded devices to wirelessly communicate to each other [32]. Further, these devices communicating directly with each other brings about new wireless channel environments to characterize. One prominent example is vehicle-to-vehicle (V2V) communications, which has application in autonomous driving research and development. Several sounding campaigns have been tailored to characterize V2V environment, such as [15, 43], with identified sounding nuances such as needing to han-

dle moving cars, lots of reflective metal in the environment, and different center frequencies [43].

Use of software defined radios in channel sounding applications has also grown in appeal with being less costly and cumbersome than more traditional architectures [52]. Channel sounders that use SDR are flexible and compact, as in [5, 9], respectively. Such flexibility within the design of sounding system which could potentially enable the use of the same channel sounder for multiple diverse applications.

Another area of interest is channel sounding efforts for exploring links for 6G communications. Terahertz (THz) frequency ranges (0.1-10 THz) have been identified to be of interest for new data-rate intensive applications emerging. Thus, channel sounding efforts have aimed at characterizing different THz propagation phenomena to aid in channel modeling. First, the free space path loss for THz communication is substantially high [38]. For THz communication, the surface roughness for objects is comparable to the signal's wavelength leading to more scattering. In [39], the mechanism of scattering in THz communications was measured and analyzed for modeling techniques. THz communications are also susceptible to molecular absorption resulting in additional losses [35]. As a result, the remainder of this thesis seeks to offer positive steps and concrete measurements examples that help towards this future use of sub-THz bands.

Chapter 3

Channel Sounding Transmitter Design with Software Defined Radios

3.1 Abstract

There is increasing need to characterize wider bands of the wireless channel as capacity needs and frequency ranges increase through channel sounding. However, equipment that can generate wideband instantaneous bandwidths for transmitting these wideband channel sounding waveforms can be cumbersome and expensive. In this paper, we explore a cost effective solution to generating GHz-wide channel sounding signals by utilizing a B210 Ettus USRP. Although this SDR has a smaller instantaneous bandwidth, it is used to transmit an FMCW channel sounding signal by retuning the radio once the current intermediate sweep has elapsed. With this method, a 1 GHz sweep is achieved with various other configuration settings to modify the structure of the sweep. Additionally, the time for retuning the B210 Ettus USRP is quantified to be 3.246 ms on average, yet the overall dwell time is dominated by GNU Radio command execution.

3.2 Motivation

Emergence of 5G and 6G communications has brought about increasing capacity needs with connecting IoT devices to the network, desired throughput requirements, and increase of high bandwidth use cases of these generations. The authors of [24] predict global mobile data traffic will grow from 130 EB per month at the end of 2023 to 403 EB per month in 2029. A significant increase in data traffic illustrates the need to both transition to higher frequency bands and utilize existing spectrum effectively.

Dynamic spectrum access (DSA) facilitates using existing spectrum more efficiently by allowing secondary users to dynamically select unused channels in a band for transmission. Typically, the secondary users will have a sensing phase that will sense currently used channels, then an active phase where an unused channel is selected for the secondary user to transmit over.

Before establishing any communications link, there need to be mechanisms to understand and characterize the wireless channel. Channel sounding can be employed to measure the channel by finding the channel impulse response (CIR) that will completely characterize a channel. Channel sounding measurement campaigns can then be used to create or validate channel models for particular environments and frequency ranges.

With communication links moving up in frequency, there have been measurement campaigns aiming to characterize the higher frequency bands with wideband channel sounding [62],[33],[70],[49],[7]. These measurement campaigns aim to gain insights into larger sections of bandwidth. While the demand for wideband channel sounding systems is increasing, some challenges exist with the implementation of wideband channel sounders, namely cost, size, and complexity of equipment.

Another area of research examines how to conduct channel sounding measurement campaigns

in DSA systems [12], [80], [48]. Conducting channel sounding evaluations in which the available spectrum and channel are adjusting requires the channel sounder transmitter to be flexible in frequency with where the transmission is located and the bandwidth of the transmission. Channel sounding conducted in DSA environments requires flexibility of the transmission bandwidth as the bandwidth available to the secondary user is dynamic. For example, [12] explores dynamically adjusting the transmit power for the channel sounding signal to a lower power if the primary user is transmitting in that band.

Due to there flexibility and accessibility, there has been research in leveraging software defined radios (SDRs) for channel sounding [52], [65], [66], [74], [3], [37]. In [3], signal restoration was explored to mitigate the challenge of SDRs introducing artifacts into the channel sounding transmission. One drawback of utilizing SDRs for channel sounding is that the SDRs do not offer large instantaneous bandwidths. The largest channel sounding system with the use of an SDR was presented in [66] at 400 MHz, being limited by the X410 USRP instantaneous bandwidth.

In this paper, we will explore creating a wideband channel sounding transmitter using a low-cost SDR in which the SDR will retune its center frequency (CF) to generate a wideband channel sounding waveform. With this retuning algorithm incorporated into the channel sounding signal, the sounder bandwidth would be limited by the transmit range of the equipment as opposed to the instantaneous bandwidth. A distinguishing factor is this channel sounding architecture will allow for plug-ins of various compatible SDRs. Additionally, the channel sounding bandwidth can be easily configured making the wideband transmitter feasible for sounding at higher frequencies and in a DSA environment. The structure of the remainder of the paper will be as follows: Section II describes the scope and setup, Section III details the design of the transmitter components, Section IV shows the validation of the transmitter design, and Section V discusses the conclusions and potential future work.

3.3 Experimental Framework

The channel sounding architecture will enable selection of available SDRs, and in this study the selected SDR is the B210 Ettus USRP. The B210 hardware has an instantaneous bandwidth of 56 MHz, though we restrict this to a usable bandwidth of 40 MHz to prevent drop off near the edge of the bandwidth range [26]. In order to achieve the desired GHz-wide bandwidth, there needs to be a mechanism to appropriately retune the center frequency of the B210 Ettus USRP.

We selected a frequency modulated continuous wave (FMCW) signal as the complex baseband channel sounding waveform. The use of FMCW for channel sounding had success in [37]-[63] and thus making the FMCW signal an appropriate channel sounding choice. The larger bandwidth is obtained by aggregating the baseband waveform modulated at different frequencies. Fig. 3.1 illustrates this retuning process to achieve a 1 GHz sweep with concatenating 40 MHz sweeps.

As shown in Fig. 3.1a, the desired bandwidth of this example is 1 GHz and it takes an arbitrarily selected time of 50 seconds to sweep through this bandwidth. However, the the baseband FMCW can be modulated up in frequency to create an intermediate sweep. Adjusting the center frequency at the end of the baseband sweep creates a transition from one intermediate sweep to another resulting in a larger overall bandwidth shown in Fig. 3.1b. Fig. 3.1c illustrates how this retuning process can be repeated to sweep through the entire desired wideband bandwidth.

In this paper, the wideband channel sounding waveform is generated by retuning a baseband FMCW sweep with a smaller bandwidth. The baseband sweep is generated using GNU Radio and fed into the B210 USRP to transmit to an IQ Recorder via a wired connection, for experimental validation. The IQ Recorder consists of a GaGe CSE123G2 12-bit digitizer

that feeds into a software that shows and records the binary samples collected called SpectraScopeRT. The digitizer can handle several configured sample rates up to 3 GS/s. Thus, the IQ Recorder will act as a spectrum analyzer to view the spectrum as well as record specific samples for playback. The set up as described above is shown in Fig. 3.2.

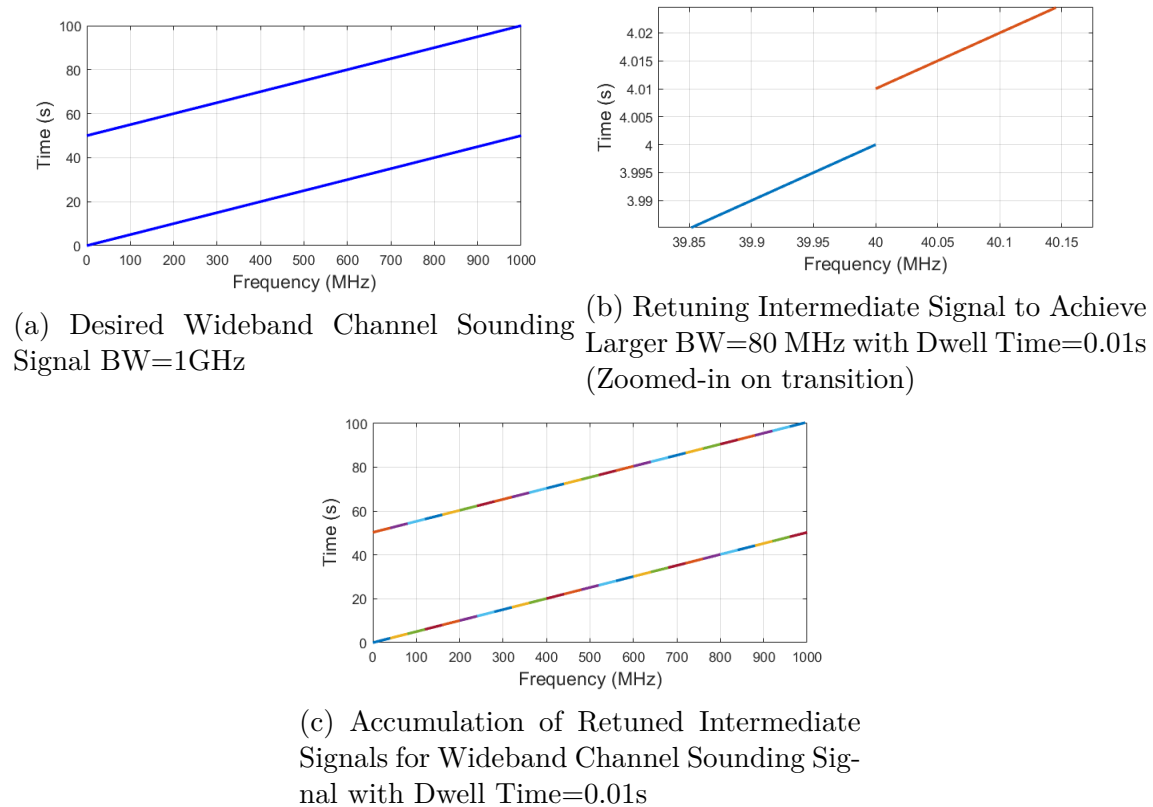


Figure 3.1: Illustration of Achieving Approximate Desired Wideband Channel Sounding Signal with Intermediate Transmissions

3.4 Design and Implementation

The elements designed for the transmitter are enclosed in the box labeled wideband channel sounding transmitter in Fig 2. The components of this transmitter are a user interface for

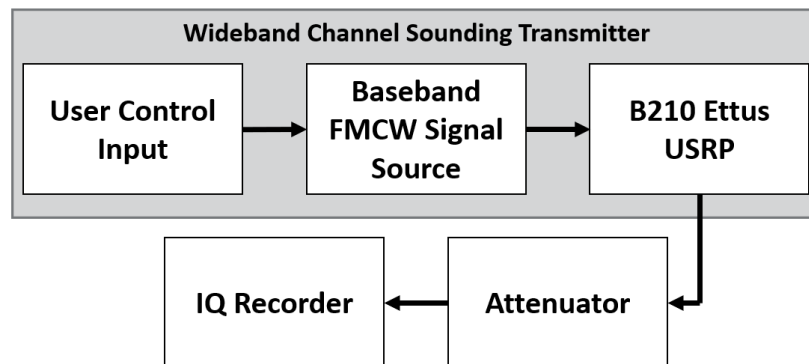


Figure 3.2: Block diagram showing the experimental setup of wideband channel sounding setting transmission parameters, a module to generate the baseband FMCW waveform, and the B210 to transmit. These elements are interfaced and controlled using a transmit (TX) manager class represented by the grey box.

3.4.1 Control Features and the User Interface

The graphical user interface (GUI) for the wideband transmitter allows for the user to customize the control settings of the transmission. The GUI is made using the PyQt library as well as QtCreator for the front-end GUI layout. Fig. 3. shows the GUI that the user interacts with to configure the settings of the transmission.

The transmission can be specified to sweep up in frequency or sweep down in frequency with respect to time by controlling the operation mode input. Another transmission configuration is the start frequency of the transmission sweep. The start frequency will be the lowest frequency in the sweep if sweeping up or the highest frequency in the sweep if sweeping down. The full bandwidth of the either frequency sweep can be specified by the bandwidth configuration.

Next, the overall slope of the transmission sweep can be adjusted by configuring the time and

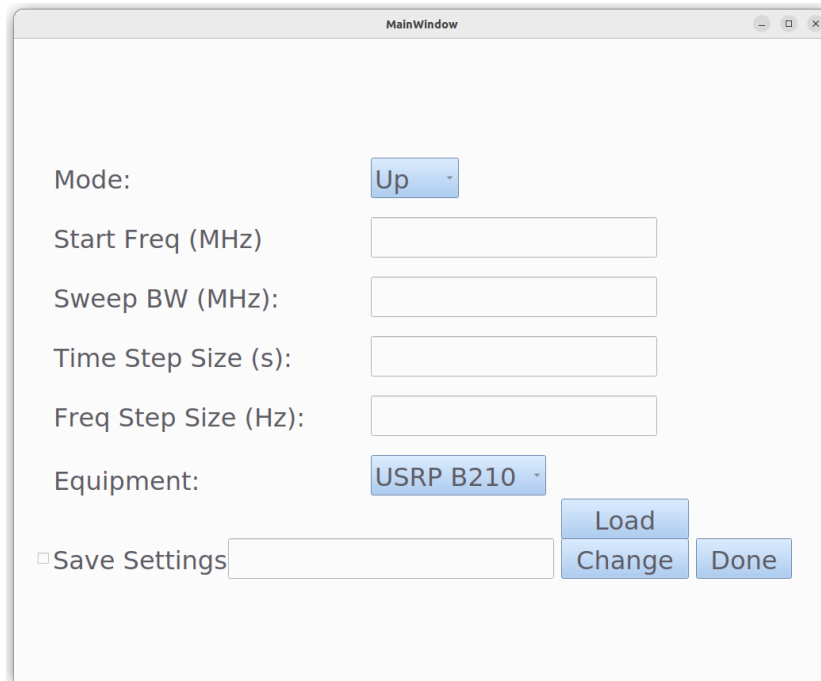


Figure 3.3: Control interface to configure the wideband transmission

frequency differential. The time differential corresponds to how much time the transmission will stay on one frequency before transitioning to the next frequency step. The frequency differential corresponds to the change in frequency for each step.

The last input relates to configuring compatible equipment to be used to transmit the channel sounding waveform. The main purpose of this section to adjust the bandwidth of the intermediate sweeps to be compatible to the chosen SDR. As such, a user is able to select a radio that they would like to use for transmitting the channel sounding waveform and the bandwidth for the smaller sweeps are set appropriately. For this study, the only possible equipment option is the B210 Ettus USRP, which has a corresponding usable bandwidth of 40 MHz.

Table 3.1 details all of the inputs the user can adjust to configure the FMCW transmission as well as their valid inputs. All of the settings that the user configures are set as member

Table 3.1: Control features for the wideband transmission, their description and possible input values

Control Feature	Description	Valid Inputs
Operation Mode	Determines the direction of sweep	Up or Down
Starting Frequency	Start of frequency of wideband transmission sweep	70 MHz-6 GHz
Bandwidth	Full wideband bandwidth of sweep	BW such that sweep is within 70 MHz-6 GHz
Time Differential	Amount of time before changing to next frequency	N/A
Frequency Differential	Step of frequency increment	N/A
Equipment	Choose what SDR is used to transmit; adjusts the intermediate BW accordingly	B210 Ettus USRP

variables in the TX manager class. The manager class instantiates the intermediate sweep module with the appropriate settings specified from the user in the GUI.

3.4.2 Baseband FMCW Waveform Generation

The component responsible for generating the actual channel sounding waveform, albeit at a shorter bandwidth, is the Baseband FMCW GNU Radio Out of Tree (OOT) Module. The OOT module generates a complex baseband FMCW signal that continuous sweeps from $-\frac{BW}{2}$ to $\frac{BW}{2}$.

In this module, a numerically controlled oscillator (NCO) drives the incrementing of the frequency over time where Δf denotes the frequency step and Δt the time step. The NCO accumulates based off of a specified step size over the phases $[-\pi, \pi]$. In this application, the stepping of the NCO represents the passage of time in discrete intervals and thus the NCO current phase can be mapped to a desired frequency. If the operational mode is "Up", then $-\pi$ gets mapped to $-\frac{BW}{2}$ and π gets mapped to $\frac{BW}{2}$ shown in equation 3.1. Alternatively, if the operational mode is "Down", then $-\pi$ gets mapped to $\frac{BW}{2}$ and π gets mapped to

$-\frac{BW}{2}$ shown in equation 3.2. The time differential is implemented by stepping the NCO after $\Delta t * f_s$ steps and the frequency differential is implemented by setting the frequency of the NCO to $\frac{2\pi\Delta f}{BW}$.

$$f_{\text{current}} = \frac{\text{NCO phase} * BW}{2\pi} \quad (3.1)$$

$$f_{\text{current}} = -\frac{\text{NCO phase} * BW}{2\pi} \quad (3.2)$$

Once the current frequency of the FMCW signal is obtained, an actual output sample is determined from a voltage controlled oscillator (VCO). The VCO takes in the current frequency, sample rate argument, and transmission power to output complex time-domain samples.

Not only is the goal of this module to create these baseband FMCW signals, but it is also designed to send a signal to the transmitter manager class when the end of the sweep has been reached. Thus, when the NCO makes a transition from π to $-\pi$, a flag is sent to the TX manager and is passed to the SDR. The purpose of this notification is to announce that the center frequency of the B210 needs to be retuned.

3.4.3 Transmitter Manager and Retuning

The three components of the transmitter are connected together using one manager class of code. The TX manager is created by modifying the generated Python code from running the GNU Radio flowgraph, which connects the baseband FMCW to a USRP Sink block. Modifying the Python code directly allows for ease in implementing dynamic retuning when prompted from FMCW OOT Module.

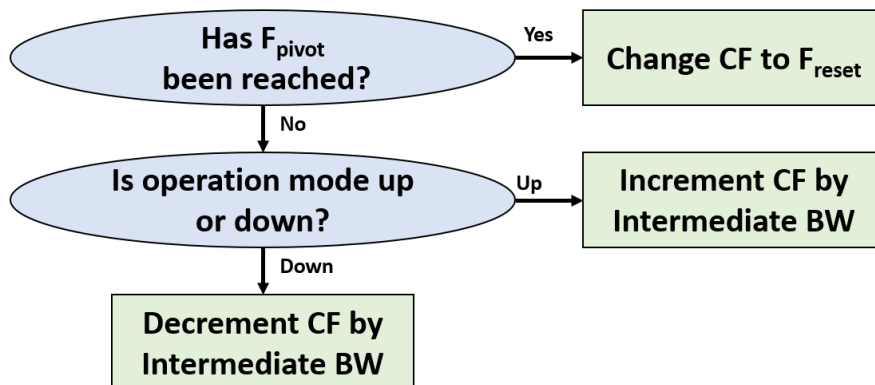


Figure 3.4: Diagram to show center frequency adjustment algorithm in TX manager

The modifications to the base Python are the addition of launching the user interface before the execution of the flowgraph as well as a function to catch the update CF signal. Launching the user interface allows for the inputs to be collected and initialized into the manager so the transmission can adjust to the user settings. The update CF signal is sent by the FMCW OOT module and when that signal is emitted, it gets caught by an added function in the manager class. This function sets the center frequency for the entire flowgraph, including the block that controls the B210 Ettus USRP, based on the algorithm outlined in Fig. 3.4. This algorithm adjusts the center frequency such that the sweep will move on to the next frequency chunk in the larger bandwidth.

Two limitations exist in the implementation of the TX manager. First, the full sweep bandwidth is restricted to being a multiple of the baseband sweep. The center frequency will only get flagged to reset at the end of an intermediate sweep and thus the full sweep will be a bandwidth that is a multiple of the intermediate sweep. The next limitation is there exists a GNU Radio command execution delay resulting from needing to check if the change CF signal has been emitted on a discrete, configurable interval. Thus, the end of the intermediate sweep occurs right after polling check, there will be the time of the period before the TX manager catches the signal and retunes the center frequency of the SDR. As a result, the

Table 3.2: Parameters for the TX Manager Effecting the Transmission

Control Feature	Input Value
Sampling Rate	30 MHz
Intermediate BW	40 MHz
GNU Radio Polling Period	100 ms

dwel time in between transmissions is the combination of the time difference from emitting the adjust frequency signal and the next execution as well as the time it takes for the SDR to change its center frequency.

3.5 Initial Validation

3.5.1 End-to-End Transmission Demonstration

In order to validate the generation of the wideband channel sounding transmission and the different possible configurations, the B210 transmitter was attached to an IQ Recorder via an attenuator. The IQ Recorder can display various visualization plots of the spectrum to validate that the sweep is located in the correct place in the spectrum. Table 3.2 shows the parameter settings that were used to in each end-to-end transmission demonstration that were configured in the TX manager.

For our demonstration, we used a 1 GHz FMCW signal from 500 MHz to 1.5 GHz to achieve this desired bandwidth. The IQ Recorder was set to have a center frequency of 1 GHz, a bandwidth of 1 GHz, and a sampling rate for the digitizer to be 3 GS/s. Fig. 3.5. show the spectrum of this transmission reaching the end of the sweep and then transitioning back to the beginning of the sweep as validation. Note that the corresponding configuration settings for this sweep are documented in Table 3.3.

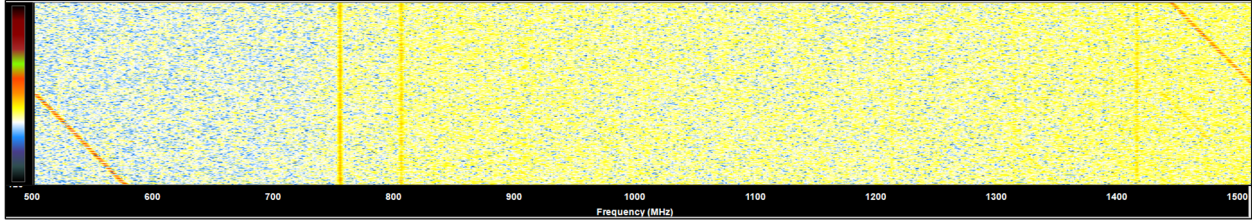


Figure 3.5: IQ Recorder waterfall plot to show end of 1 GHz frequency sweep n (right hand) and the start of sweep $n+1$ (left hand)

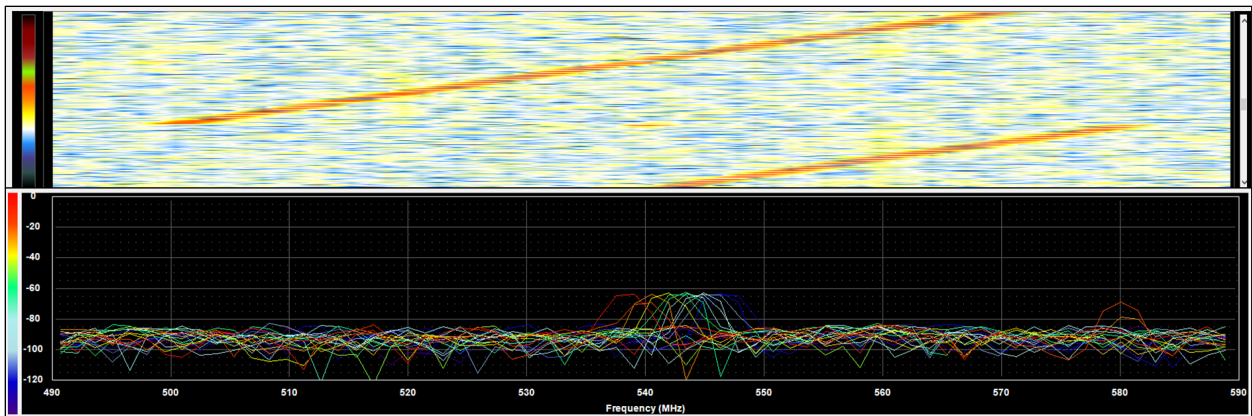


Figure 3.6: IQ Recorder waterfall plot and persistence plot to show 80 MHz down sweep

Table 3.3: Transmission settings corresponding to the frequency sweep shown in Fig. 3.5.

Control Feature	Input Value
Operation Mode	Up
Starting Frequency	500 MHz
Bandwidth	1 GHz
Time Differential	Default
Frequency Differential	Default
Equipment	B210 Ettus USRP

Table 3.4: Transmission settings corresponding to the frequency sweep shown in Fig. 3.6.

Control Feature	Input Value
Operation Mode	Down
Starting Frequency	500 MHz
Bandwidth	80 MHz
Time Differential	67ns
Frequency Differential	1 Hz
Equipment	B210 Ettus USRP

Another transmission was performed at a smaller full sweep bandwidth in order to illustrate the entire sweep with one validation plot. Fig. 3.6 shows a channel sounding transmission of 80 MHz sweeping down in frequency which illustrates the ability to retune the center frequency to achieve a large bandwidth. The IQ Recorder settings included having a center frequency of 540 MHz, a bandwidth of 80 MHz, and a sampling rate of 3GS/s. Table 3.4. details the settings for this demonstration sweep.

3.5.2 Quantifying Dwell Time

We quantify the dwell time by utilizing the IQ Recorder to make a recording of the spectrum of the transition from one intermediate sweep to the next. The recorded binary data of the transmission can then be processed in SpectraViewRT, the playback software on the IQ Recorder to determine the lapse between the end of an intermediate transition to the start of the next one. Table 3.5 shows time delays associated with command execution as well as time delay corresponding to the SDR retuning for testing iterations.

The average overall dwell time was calculated to be 33.521 ms with main component of the dwell time attributed to a delay between emitting the adjust CF signal and the next timer interrupt. Although the maximum GNU Radio command execution delay was found to be

Table 3.5: Dwell time measurements

GNU Radio Command Execution Delay (ms)	Retuning Delay (ms)	Overall Delay (ms)
44.393	3.094	47.487
36.1502	3.327	39.477
10.283	3.317	13.6

44.393 ms, the delay could be as large as the GNU Radio polling time. The GNU Radio polling time for these tests were 100ms, so the overall delay could be about as larger as 100 ms plus retuning delay. Due to the random nature of the command execution delay the dwell time should be modeled as a random variable with a uniform distribution between the retuning delay to the retuning delay plus the timer period. In this test case, the dwell time would be $t_{\text{dwell}} \sim U(3, 103)$ [ms] with the expected dwell time being about half the polling time.

3.6 Conclusions and Future Work

This research aims to create a cost effective solution to transmit a wideband channel sounding waveform to characterize the wireless channel using SDRs. A wideband channel sounding transmitter is created using a B210 Ettus USRP that periodically retune to create a wideband FMCW transmission out of intermediate smaller bandwidth sweeps. Through this method, a 1 GHz sweep is achieved sweeping from 500 MHz to 1.5 GHz. This transmitter can be configure using the GUI to sweep up or down in frequency, select where the sweep is located in spectrum, as well as change the slope of the sweep. The dwell time in between the intermediate transmission is dominated by the command execution delay, and thus the overall expected dwell time is about a half of the GNU Radio polling time. With more powerful

computing, the expected dwell time could be as low as 5 to 10 ms with the retuning delay being more significant facet of the overall delay. The successful transmission and relatively small dwell time shows that SDRs can be used to be a promising solution to low cost and low complexity wideband channel measurement campaigns. Additionally, with the ability to easily adjust the full transmission bandwidth, this transmission architecture could be compatible with sounding within DSA environments where frequency agility is required.

Future work will focus on incorporating additional SDRs to be configured to use for transmitting the wideband channel sounding signal. A map can be created to configure the intermediate sweep bandwidth to be a usable bandwidth for the chosen piece of equipment. Being able to configure the SDR would increase the flexibility of this program to interface with various pieces of equipment.

Another modification that can be incorporated into the channel sounding transmitter software is to change the type of waveform that will be used for channel sounding. In this study, a FMCW signal is used for exciting the channel, but another waveform could be used to gauge the channel and glean additional information. For example, pseudo-random noise (PN) can be used as the channel sounding waveform as PN is used with correlation-based channel sounders. The same technique explored in this paper can be used to retune to the next frequency section after the sounding has occurred in the intermediate bandwidth to accumulate and achieve a larger channel sounding bandwidth.

In addition to modifications to the actual channel sounding transmitter, the natural next step is to apply the channel sounder transmitter to measure the channel. The wideband channel sounding waveform would be transmitted over the air to observe the wireless channel and post processing to extract channel characteristics. The received signal from this channel sounding waveform can then be used to create meaningful measurements of the wireless channel.

Chapter 4

Waveform Selection Comparison

4.1 Abstract

Collecting measurements of the wireless channel through channel sounding campaigns is an important step to gauge operational constraints on a communications system. With the advent of higher frequency bands in mmWave and sub-terahertz for 5G and future 6G technologies, there are an ever-increasing number of devices communicating with each other under new channel environments that require characterization. Popular methods to sound the channel include either utilizing a vector network analyzer or observing the channel impulse response directly from the processing of a known channel stimulus waveform. Further, when exciting the channel directly from a known stimulus waveform, there is appeal in using software defined radios (SDRs) for flexibility and accessibility. Given that the choice of the waveform affects the sounding capabilities of a system, it is important to understand and characterize the trade-space of each of the waveforms for sounding efforts, particularly sounding in different environments. In this chapter, we investigate the performance of utilizing various stimulus signals within context of using low-cost radios for channel sounding to provide three contribution: (1) theoretical performance analysis based off of baseband waveform and processing algorithm properties, (2) system design for channel sounding transceiver with a low-cost radio transmitter, and (3) validation of system with sounding measurements equipped with frequency retuning.

4.2 Motivation

Channel sounding is a technique to characterize the effects the channel propagation environment has on wireless communication signals by exciting the environment to estimate the channel impulse response (CIR). Measurement campaigns can be used to develop statistical models of propagation characteristics and to generate data to validate theoretical channel models. An understanding of the channel plays an important role in developing constraints for the operation of communications systems. Channel sounding research is moving towards mmWave (mmW) and sub-terahertz frequencies for 5G and 6G communication systems to access higher data rates for bandwidth intensive applications. Compared to lower frequencies, there are additional physical phenomena that affect the propagation of a higher frequency mmW signals. Examples of such phenomena include penetration losses [40], atmospheric attenuation [50], and human blockage [55]. 5G also enables the connectivity of Internet of Things devices through sidelink communications, offering new channel environments to characterize. Two specific cases are measuring angle of arrive and Doppler shifts in Vehicle-to-Vehicle (V2V) communications [15] and real-time doppler shift measurements in factory automation environments [27]. While interested in channel sounding at these mmW frequencies, this paper seeks to develop a frequency-agnostic evaluation of the underlying baseband sounding waveforms.

One method of conducting channel sounding involves utilizing a vector network analyzer (VNA) to collect measurements of the transfer function of the channel, then obtaining the CIR by applying the inverse Fourier Transform on the measurements [34]. Another approach measures the CIR directly from the reception and processing of specific (usually pulse compressed) excitation signals [64]. Despite requiring custom equipment and processing, the direct transmission approach is an appealing choice for future sounding campaigns since it can collect measurements in real time but does not require a direct connection [34].

Traditional channel sounding architectures are quite cumbersome, inflexible (with adjusting sounding frequency), and expensive [52]. Areas of research have been dedicated to mitigate these issues by employing software defined radios (SDRs) in channel sounding systems [27], [52], and [41]. Use of SDRs can have a range of advantages, including making the channel sounding system as lightweight and compact as possible in embedded applications [9], to creating an extremely flexible channel sounder [5]. Despite the flexible use of SDRs, there are some drawbacks in using them for channel sounding applications. Limitations included low sampling rates that lead to small instantaneous bandwidths, limited center frequency ranges, limited receiver dynamic range, and hardware imperfections that vary from device to device [79]. If sounding at higher frequencies, the limited RF front ends on the SDRs would necessitate the use of additional RF upconversion which can lead to additional efforts calibrating RF variations between the SDR and RF converters.

In generating each of these waveforms as well as comparing to different existing campaigns, coming up with universal comparisons between the sounding capability from utilizing the various waveforms can be difficult. While looking at previous campaigns is helpful, this exploration does not lend to a direct source of comparison due to differing conditions, assumptions, and environments under which the previous campaigns were performed. Some direct comparisons do exist: In [71] the OFDM sounding method was analyzed with different modulated sequences including, binary pseudo-random noise (PN), random, and Zadoff-Chu and found that the Zadoff-Chu sequence allowed for the detection of the most multipath components (MPCs). Three spread sounding signals (PN, Gold Code, and Zadoff-Chu) used to collect measurements and compared in [52]. The swept-time direct cross correlation (STDCC) method and the OFDM method were compared in [72] with the STDCC method performing better, but improved performance attributed due to bandwidth limitations. However, these cases do not examine different scenarios that might require different

channel sounding needs.

In [55], different hardware post processing architectures are outlined and implemented to process the same waveform type (PN) for different sounding performance advantages. One of the cases is the sliding correlator architecture, first introduced by [16], which implements the post processing algorithm in the analog domain correlating the received signal with a slightly slower sequence. This processing technique results in a bandwidth compressed channel estimate that eases the ADC sampling rate requirements. The main disadvantage of the sliding correlator system is a decreased Doppler resolution due to the time in between channel measurements being proportional to the slide factor [60]. The decrease in Doppler resolution motivates a second hardware architecture in [55], in which the received signal is directly sampled and processed in the digital domain.

The contributions made in this paper can be summarized into three categories: (1) analyze performance constraints stemming from selection baseband waveform and processing technique (2) detail a system design for conducting sounding on low-cost SDRs, and (3) demonstrate the proposed channel sounding system with frequency retuning to collect measurements at 950 MHz. In contribution (1) we perform a qualitative analysis of five different channel sounding waveforms and three different post processing methods in the context of channel sounding with low-cost SDRs. Comparisons in theoretical performance for each waveform inform recommendations for waveform selection. In contribution (2) we design a hardware architecture and software processing for conducting wideband channel sounding through retuning a low-cost, narrowband SDR transmitter. In contribution (3) we demonstrate the realized sounding system with power delay profile measurements collected across 120 MHz bandwidth using 40 MHz intermediate transmissions. Further, the demonstration of frequency retuning validates the flexibility of the architecture to perform channel sounding over larger bands of operation.

These contributions aide in considering the trade-space of choosing a particular sounding waveform, along with considering their associated digital post processing algorithm. Novel to this paper is the consideration of explored trade-space to make informed waveform recommendations based off of channel sounding scenario. While hardware architectures play a role in sounding performance, we will be focusing on performance of each waveform within the context of utilizing a low-cost SDR transmitter and directly sampling the RF for processing offline, largely identifying and optimizing around the constraints of low-cost SDR hardware, rather than proposing other hardware architectures. When comparing each of the waveforms, the following performance metrics are considered to gauge holistic sounding performance from factors that influence ability to accurately characterize the channel to performance within the context of low-cost SDR systems:

- Temporal Resolution
- Maximum Recoverable Excess Delay
- Doppler Resolution
- Computation Complexity
- Ease of Implementation
- Peak to Average Ratio
- Over the Air Performance

The remainder of the paper is structured as follows: Section II contains a detailed analysis of each waveform being considered and performance metrics that are derived from the construction and processing implementation from each waveform. Section III provides details on a flexible channel sounding platform using an Ettus USRP B210 SDR that will facilitate the

comparison between sounding waveforms. Section IV discusses the results of sounding measurements taken at 950 MHz and details various channel sounding scenarios with waveform recommendations. Section V summarizes waveform performance across sounding metrics, showing that waveform selection is situational, yet leans toward Zadoff-Chu sequences for most applications.

4.3 Baseband Waveform Selection and Comparison

The CIR of a time varying multipath channel can be viewed/modeled in the form of the discrete impulse equation 4.1, representing a collection of (k) Multipath Components (MPC).

$$h(\tau, t) = \sum_{k=1}^N \alpha_k(t) e^{j\phi_k(t)} \delta(\tau - \tau_k(t)), \quad (4.1)$$

where the t represents the instance of time the channel snapshot was taken, τ represents the delay from the LOS component, and $\alpha_k(t) e^{j\phi_k(t)}$ is the complex strength with amplitude $\alpha_k(t)$ and phase $\phi_k(t)$ of the k^{th} MPC which occurs at delay $\tau_k(t)$. Observe the use of discrete-time notation as motivated by representing the multipath channel as a set of time-shifted, phase-rotated echos of the transmitted signal that are received [61]. Also, note the inclusion of the dependence of time the snapshot was taken in the representation for each MPC. Fig. 4.1 shows a visualization of the Time Varying channel taken at snapshots in time. For a static channel, the equation loses the dependence of time as shown in Eqn. 4.2

$$h(\tau) = \sum_{k=1}^N \alpha_k e^{j\phi_k} \delta(\tau - \tau_k) \quad (4.2)$$

Again, the goal of broadband channel sounding is to use the reception of a waveform $x(t)$

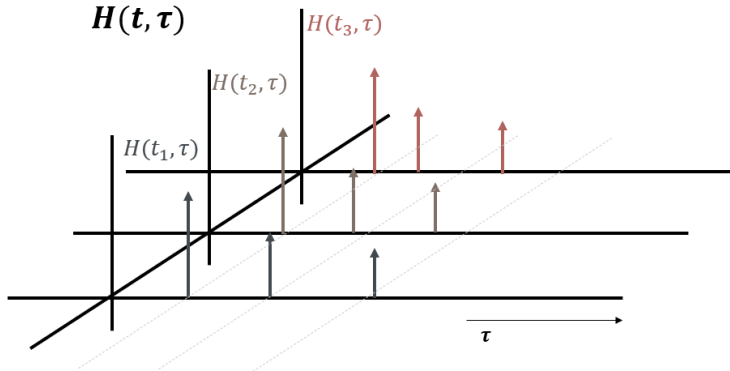


Figure 4.1: Visualization of Discrete Time-Varying Channel

to estimate the response of the channel described in Eqn. 4.1. Once the CIR estimate (snapshot) is obtained in the time domain, the MPCs can be extracted from peaks in the CIR with associated time delays and strengths to fit the form of Eqn. 4.1 and 4.2.

4.3.1 Channel Sounding Waveforms

The waveforms selected for comparison are direct pulse, PN, Zadoff-Chu, Frequency-Modulated Continuous Wave (FMCW), and Orthogonal Frequency-Division Multiplexing (OFDM) multi-tone based on prevalence in sounding campaigns. Table 4.1 shows each of the waveforms as well as configuration parameters that dictate how an instance of these waveforms are generated which will be discussed further in the below section. Fig. 4.2 shows each of these waveforms in the time and frequency domains, which also illustrates how some of these configuration metrics manifest.

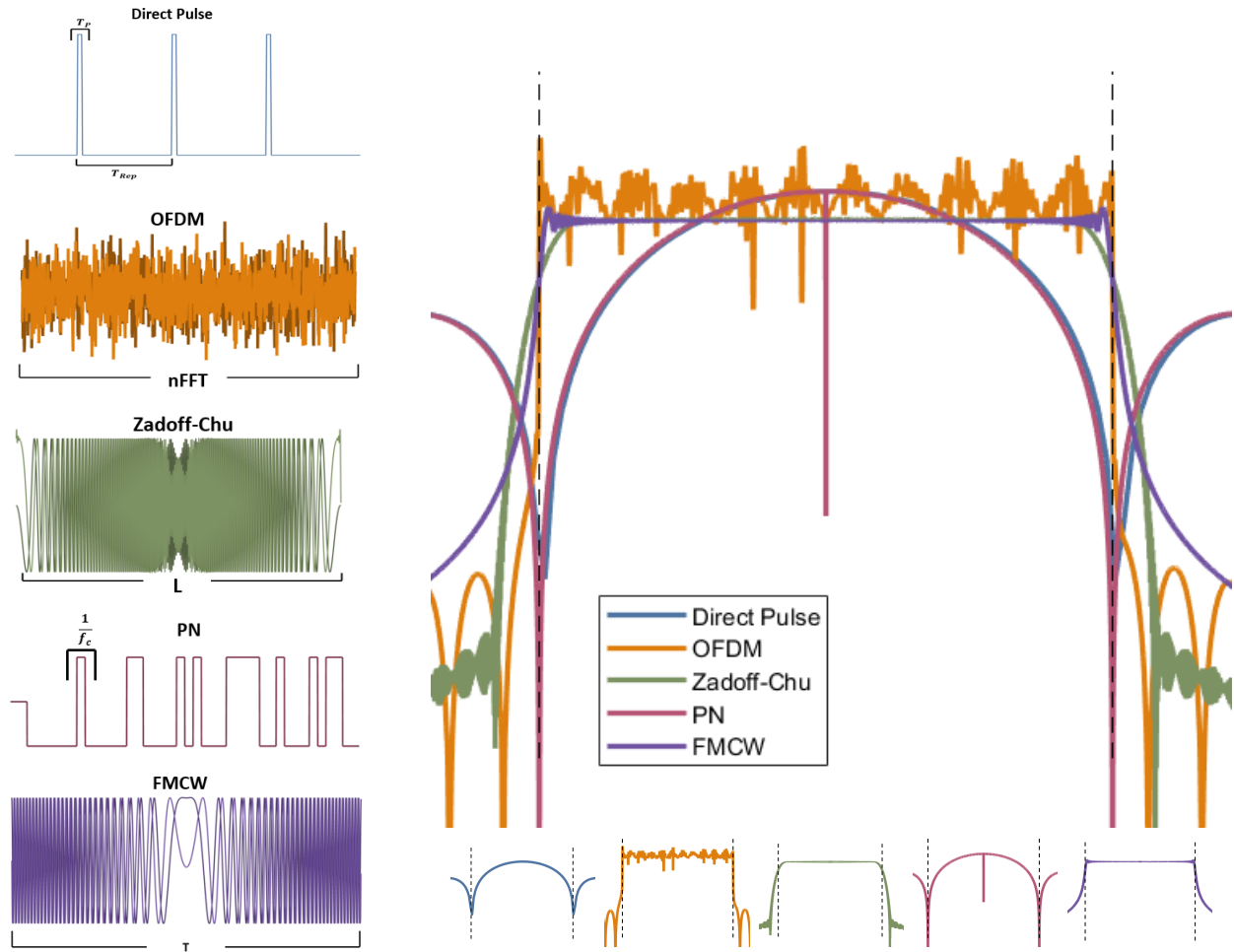


Figure 4.2: Time and Frequency Domain Representations for Channel Sounding Waveforms

Direct Pulse

The direct pulse is a train of short pulses that sufficiently resemble the Dirac Delta function. As shown in Fig. 4.2, the rectangular pulse shape of the baseband signal corresponds to a frequency domain representation with sidelobes containing significant out-of-band energy.

Frequency Modulated Continuous Wave

The bandpass equation for the (linear) FMCW signal is show in Equation 4.3 [64].

Table 4.1: Waveform Configuration Parameters that Inform Signal Generation

Waveform	Configuration Parameter 1	Configuration Parameter 2
Direct Pulse (train)	Pulse Duration (T_p)	Pulse Spacing (T_{REP})
FMCW	Duration (T)	Bandwidth (BW)
Zadoff-Chu	Sequence Length (L)	Bandwidth
PN M-Sequence	Number of Shift Registers (N_{sr})	Chip Rate (f_c)
OFDM	Number of Subcarriers (n_{FFT})	Bandwidth

$$x(t) = \cos \left(2\pi f_c t + 2\pi \frac{BW}{2T} t^2 \right) \quad (4.3)$$

As shown in the time domain representation in Fig. 4.2, the FMCW waveform has a set bandwidth (BW) that sweeps across the duration (T), giving rise to the sweep rate (BW/T) and dispersion factor (BW*T). In order for 98% of the signal's energy contained within the band of interest, the dispersion factor must be larger than 100 [64]. Naturally, this limitation defines a lower limit on the duration of the sweep for a given bandwidth.

Binary Pseudo-Random Noise (PN) Sequence

Another pulse-compressed waveform is the binary pseudo-random noise (PN), which is designed to exhibit behavior that appears random. The most common generation of these PN sequences comes from loading N_{sr} shift registers with an initial state, shifting out register values into the sequence and applying a feedback polynomial to load the first register [60]. A special case of these sequences is called the maximal length sequences (m-sequences) in which the polynomial selected such that the sequence can achieve a period of $2^{N_{sr}} - 1$. As with the case of the direct pulse, the rectangular pulse shape of the signal will lead to a frequency domain representation that exhibits excess leakage into the neighbor bands.

Zadoff-Chu Sequence

Unlike the PN signal generated from a binary spreading signal, the Zadoff-Chu sequence falls under the class of polyphase spreading signals. The Zadoff-Chu sequence is a constant amplitude zero autocorrelation (CAZAC) sequence meaning that it optimally samples the unit circle to obtain a sequence. The Zadoff-Chu pulse can be generated with equation 4.4 [41]:

$$x[n] = \exp\left(-j\pi u \frac{n(n+1)}{L}\right) \quad (4.4)$$

in which u is an odd root-of-unity value, and L is the length of the sequence. For proper generation, the root value and the length of the sequence must be co-prime.

Multi-Tone OFDM

In general, multi-tone sounding signals are composed of a collection of tones spaced out among sounding bandwidth. Channel sounders that uses the multi-tone waveform often intentionally set the phases of the each of the sinusials to lower the crest values and peak to average power (PAPR) ratio [10]. A specific case of this class of signals is the OFDM packet that is completely composed of known pilot tones. The time-domain representation of the OFDM multi-tone signal is show in Equation 4.5 [5]:

$$x[n] = \sum_{k=-\frac{\text{nFFT}}{2}}^{\frac{\text{nFFT}}{2}-1} X[k] \exp\left(\frac{j2\pi kn}{\text{nFFT}}\right) \quad (4.5)$$

in which $X[k]$ is modulated known symbols and appropriately set to zero on the outer bands to maintain the bandwidth of the signal.

4.3.2 Processing Techniques

The three general categories we will be considering for obtaining the channel estimation from the received signal based on the waveform chosen include: direct, correlative, and frequency-domain.

Direct

One of the simplest channel sounding designs in concept is to transmit a pulse that sufficiently resembles the Dirac Delta function. The only excitation signal that can be used for this processing technique is the direct pulse train. The direct approach is simply to take the received signal as a scaled version of the channel response used in the direct pulse method. Mathematically, this is simply $x(t) \approx \delta(t)$, thus $y(t) = (x * h)(t) \approx h(t)$.

Correlative

A correlative receiver can be used for processing received pulse compressed signals, whose autocorrelation function resemble a Dirac Delta function. In this approach, the channel response can be estimated by correlating the sent pulse with the received pulse, as shown below.

$$y(\tau) = (x * h)(\tau) = \sum_{k=1}^N \alpha_k e^{j\phi_k} x(\tau - \tau_k)$$

from Eqn (2) and with $x \star x \approx \delta(\tau)$, with \star being the notation for correlation

$$x \star y = x \star \sum_{k=1}^N \alpha_k e^{j\phi_k} x(\tau - \tau_k)$$

$$\begin{aligned} &\approx \sum_{k=1}^N \alpha_k e^{j\phi_k} \delta(\tau - \tau_k) \\ &\approx h(\tau) \end{aligned}$$

in which \star denotes correlation, $*$ denotes convolution, and $x \star x \approx \delta(\tau)$. The pulse compressed waveforms that we will be exploring in this paper is the FMCW, PN signal, and Zadoff-Chu signal.

Frequency Response

In the OFDM packet structure, there are designated pilot tones that are transmitted to gauge the channel in real-time. The processing of these known pilots involves leveraging the relationship between the frequency domain of the received signal and transmit signal to obtain the channel response. Mathematically, this is simply $H = Y/X$, where H is the channel transfer function and Y and X are the FFT of the receive and transmit signals, respectively. The results of the equalization terms calculated from the pilot tones is then extrapolated to the communications subcarriers within the context of a communications system. The frequency-domain method of determining the FFT of the received signal and dividing by the frequency response is not exclusive to the OFDM method of sounding and has been used in [55] and [41].

4.3.3 Channel Estimation Technique Performance

Temporal Resolution

The temporal resolution measure defines the smallest separable time delay between MPCs. In all cases, the temporal resolution is related to the bandwidth of the transmitted signal. For the direct method of channel estimation, the temporal resolution is simply the duration of the transmit signal. In both the correlative and the frequency domain cases, the temporal resolution's dependence on bandwidth comes from the relationship between the frequency spectrum and the autocorrelation function. Channel sounding signals that are complex-valued have a temporal resolution of $\frac{1}{BW}$, while real value sounding signals have a temporal resolution of $\frac{2}{BW}$. Thus, the FMCW, Zadoff Chu, and OFDM signals have a temporal resolution of $\frac{1}{BW}$ and the PN signal has a temporal resolution of $\frac{2}{BW} = \frac{1}{f_c}$, with f_c being the chip rate.

Maximum Recoverable Excess Delay

Maximum recoverable excess delay is a measure of the largest delay that can be measured from a sounding system. Regardless of the transmit waveform case, this metric will depend on the period of the waveform being emitted. Thus, this metric is less of a point for comparison and more so a noteworthy performance metric that would need to be accounted for in a sounding design. In most cases, the period of the waveform is the duration of the signal, assuming there is no retransmission timing gaps.

Doppler Resolution

The maximum Doppler shift that sounding measurements can achieve is dependent on the rate at which the channel is measured by the Nyquist theorem. The rate at which these snapshots can be taken is dependent upon the hardware architecture used for the sounding campaign and not necessarily the waveform or processing algorithm. Note that increasing the duration of a signal will yield a larger maximum recoverable excess delay but will lead to a smaller doppler resolution.

Computational Complexity

The direct reception method is the most computationally efficient as the estimate is obtained immediately at reception of the signal. The frequency domain method is the next most efficient post-processing algorithm that can be performed in real-time for a system, with FFT having a computation complexity of $O(N \log_2 N)$ [45]. The most time consuming for processing of the sounding waveforms is the direct correlative receiver with a computation complexity of $O(N M)$.

Ease of Implementation

In this context utilizing SDRs, the IQ samples for each waveform get directly sent to the SDR for transmission making transmitter implementation identical among the waveforms. Thus, it makes more sense to consider the ease of implementation of each of the processing algorithms for the waveforms in terms of post processing steps. The direct pulse case requires little processing upon reception since the premise is to directly observe the channel, making it the easiest to implement. Next, the correlative method only has one additional operation of correlation before obtaining the channel estimate. The most involved method in terms of

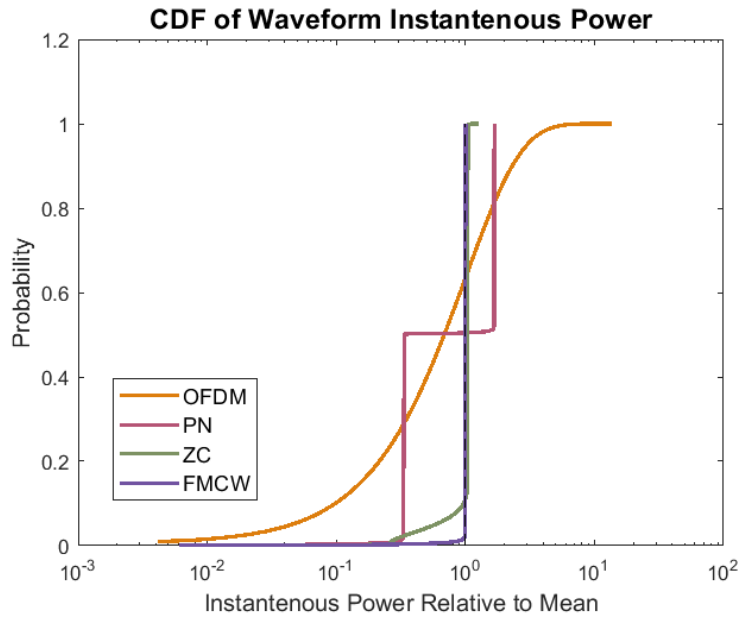


Figure 4.3: Instantaneous Power Distributions for Five Repetitions of Each Sounding Waveform with Power Fade in Filter Applied

number of steps for implementation is the frequency domain method.

Peak to Average Power

Since the max power of a signal should avoid compressing the power amplifier, a high peak-

Table 4.2: Instantaneous Power Distribution Statistics

Waveform	PAPR (dB)	Skewness	Kurtosis
Direct Pulse (train)	7.93	5.23	29.75
FMCW	0.018	-12.48	170.97
Zadoff-Chu	0.98	-3.69	15.99
PN M-Sequence	1.45	0.02	1.00
OFDM	10.28	2.01	9.17

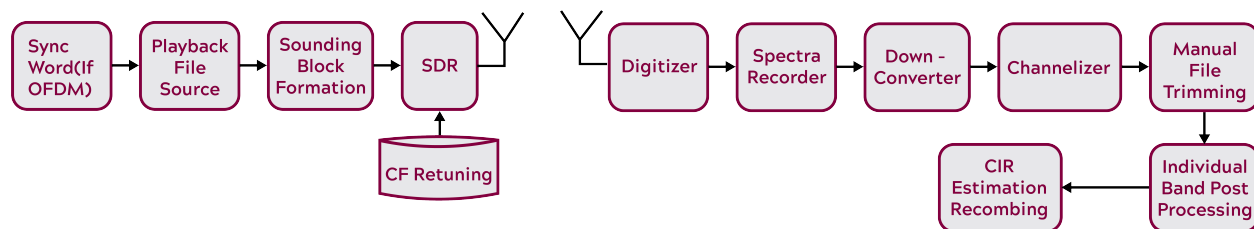


Figure 4.4: Channel Sounding Transceiver Block Diagram

to-average power ratio (PAPR) requires additional back off in power. For low-cost SDRs, this leads to a lower potential dynamic range available to the measurement system. Fig. 4.3 shows the cumulative distribution functions (CDFs) of the instantaneous power of each of the waveforms centered around the mean instantaneous power for that waveform. The direct pulse train estimating the Direct Dirac function is not included in Fig. 4.3. because the low duty cycle does not lend itself to visualization on the log-scale CDF. From Fig. 4.3 and Table 4.2, we can see that the OFDM and Direct pulse cases have the highest peak to average power ratio and the FMCW and Zadoff-Chu signals have the lowest peak to average power ratio. Further, both the FMCW and Zadoff-Chu are the only signals to have negative skewness, which indicates that the power distribution favors the higher instantaneous power values, which is desirable in this context. The larger kurtosis value for the FMCW, Zadoff-Chu, and direct pulse cases are indicative of these distributions having values concentrated towards the mean. For the FMCW and Zadoff-Chu this behavior is due to being at a constant power while in the direct pulse case is due to a small duty cycle.

4.4 Experimental Setup

Fig. 4.4 details the full hardware setup of the sounder. Measurements were taken at a center frequency of 950 MHz with the use of two omnidirectional flat panel antennas[46]. The transmitter design is an updated design from [28], which utilizes center frequency re-

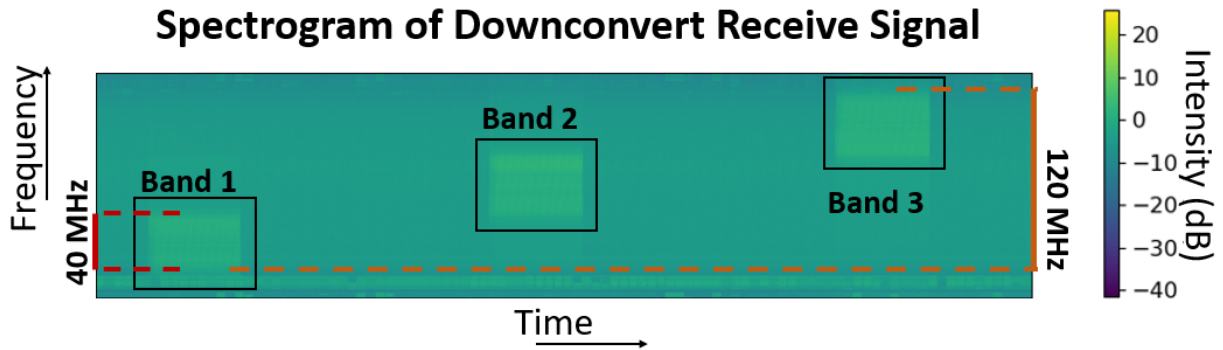


Figure 4.5: Baseband Received Spectrogram showing Channel Sounding Blocks at Various Center Frequencies

tuning of an Ettus USRP B210 to achieve a larger transmit bandwidth. Improvements have been made where instead of continuously generating the same waveform (FMCW) using a custom-built GNU Radio Out-of-Tree module, the transmitter accepts a playback file for the baseband sounding signal. Each of the waveform playback files have been normalized to the same aggregate energy, approximate duration, and intermediate bandwidth of 40 MHz (except for PN and Direct with 33.4 MHz; see Low-Cost Hardware Considerations Section III.A). Table II details the achieved waveform configuration parameters used for measurement collection. The samples read from the playback file are repeated 100 times to form a so-called channel sounding block. Once the full block has been transmitted from the Ettus USRP, the frequency retuning algorithm [28] adjusts the center frequency that the USRP is transmitting on. In our case, this was a total of three retransmits to achieve a combined bandwidth of 120 MHz. With this setup, the dependency on GNU Radio (and using the custom module) is replaced by utilizing Python's UHD library. With this method, the dwell time between intermediate transmission is dependent only on the dwell time for frequency retuning the B210 instead of also including an additional delay.

On the receive side, the RF is directly sampled off into a raw data file for receiving and post processing in software offline. The receive antenna is directly connected to an IQ

Recorder (Vitretek EON CSE123G2 Signal Recording System [77]), which contains a GaGe CSE123G2 12-bit digitizer with a sample rate of up to 3 GS/s, a spectrum recording software (SpectraScopeRT), and 38.4 TB in RAID storage. With no additional RF processing, the digitizer's sample rate limits maximum frequency that can be recorded to 1.5 GHz. A recording of the channel can be made without synchronization between the transmitter and receiver due to a manual file trimming step made in software. The recorded data files are transferred back to the PC that houses the transmitter for processing and channel impulse response estimation. Like the transmitter, the receiver has a flexible design in which the center frequency, bandwidth of signal, and number of channels can be specified on reception based on what was transmitted. An example received spectrogram is shown in Fig. 4.5, which shows the intermediate channel sounding blocks on three different channels. The receiver software will downconvert the raw recorded samples based on the center frequency, filter and decimate the signal based on full bandwidth, and lastly apply a channelizer to isolate each intermediate channel sounding block. Manual file (course) trimming is then applied to each of the channelized files such the channel sounding blocks are isolated. An additional mode of operation does not require the manual file trimming with course synchronization from a wired Ethernet connection between the transmitter and receiver. The resulting output of the receiver is a complex baseband data file for each of the bands configured by the transmitter containing received channel sounding blocks for post processing.

$$CIR = \begin{bmatrix} h(t_1, \tau_1) & h(t_1, \tau_2) & \dots & h(t_1, \tau_N) \\ h(t_2, \tau_1) & h(t_2, \tau_2) & \dots & h(t_2, \tau_N) \\ \vdots & \vdots & \ddots & \vdots \\ h(t_{N_R-1}, \tau_1) & h(t_{N_R-1}, \tau_2) & \dots & h(t_{N_R-1}, \tau_N) \\ h(t_{N_R}, \tau_1) & h(t_{N_R}, \tau_2) & \dots & h(t_{N_R}, \tau_N) \end{bmatrix} \quad (4.6)$$

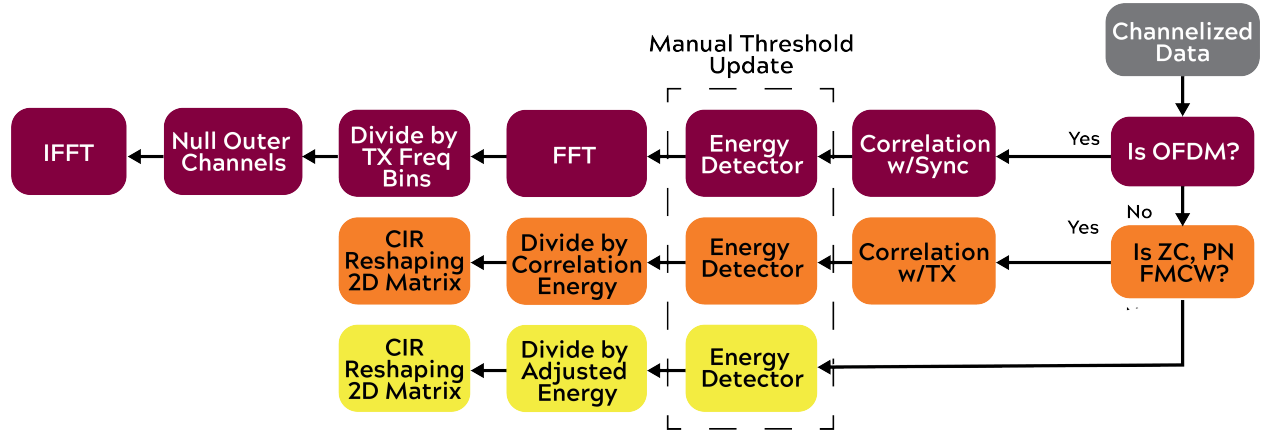


Figure 4.6: Post Processing Algorithm by Waveform Block Diagram

The goal of the post processing, regardless of the waveform, is to take the received channelized data file that contains the received channel blocks and generate a channel impulse response estimate block. The CIR response takes the form of the matrix shown in Eqn. 4.6, where N is the number of samples within a period of the channel sounding waveform, and N_R is the number of repetitions within one channel sounding block ($N_R = 100$ for this setup). In this representation, the rows of the channel impulse response block represent the CIR estimated at a specific time, whereas the columns represent the delays. Note that in our receiver architecture one pass through the receiver and post processor can generate multiple CIR blocks for each channel depending upon the manual file trimming.

Fig. 4.6 provides a high-level diagram of the processing algorithms that each of waveforms undergo to obtain the channel impulse response block. For each waveform, each of the channelized data files are read in as serial receive data and are synchronized to the start of the received channel sounding block with the utilization of an energy detector with a manual set for the energy threshold. For the correlative post processing method, used for the FMCW, PN and Zadoff-Chu waveforms, the serial received data is correlated with the transmitted receive data to directly yield the serial CIR estimate and then feed into the energy detector for detection. Once the start of the serial CIR is detected, it is simply reformatted into the

channel impulse response block form. For the direct post-processing method, the approach of the processing algorithm is similar, just without the correlator. The serial received data for each of the channels directly goes through the energy detector until the serial CIR is detected and reformatted into the CIR blocks. Unlike the other cases, the frequency domain algorithm utilizes a sync word for synchronization and thus the serial received data is first correlated with the sync word and then fed into the energy detector. From this point the received channel block can be isolated in the serial received data and is processed n_{FFT} -length buffer windows. The current buffer of n_{FFT} samples will go through an FFT operation, element-wise division with the known frequency symbols, nulling of exterior sub-channels outside the bandwidth of the signal, and last an IFFT operation to obtain that time instance's CIR estimate. The buffer's CIR estimate is directly loaded into the rows of the channel impulse response blocks. Once each channelized data file has been processed and the corresponding CIR estimate blocks have been generated, the different channel blocks get combined to increase temporal resolution performance using frequency domain concatenation. Note that successful combining through frequency domain concatenation is possible, even though the phase is discontinuous transitioning from one intermediate transmission to the next retune as detailed in [85]. Power delay profile can be determined through averaging the CIR estimate blocks across time.

4.4.1 Low-Cost Hardware Considerations

Utilizing an SDR for a channel sounder has numerous advantages, accessibility and flexibly to name a few, but they also introduce constraints into the system that could limit performance if not addressed. One such limitation is the oft times small instantaneous bandwidth capabilities for the equipment. The Ettus USRP B210 is the SDR used for collection of measurements in this paper's experiments, which has an instantaneous bandwidth of 56 MHz.

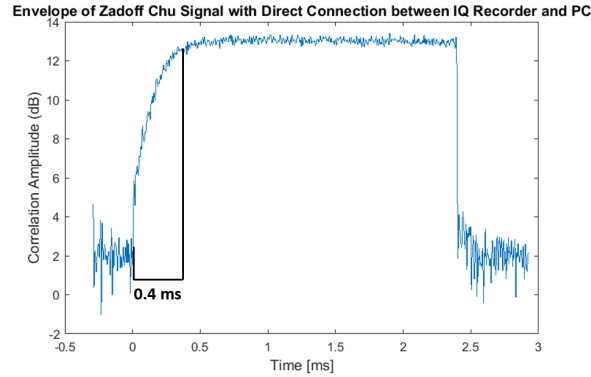


Figure 4.7: Envelope of USRP RF Front End Filter Transient Response with Each of the Waveforms

Given the wideband requirements for future sounding campaigns, these small bandwidths are not suitable for channel sounding. A method to mitigate the low instantaneous bandwidth is to implement a frequency retuning algorithm to sweep through a wider bandwidth, as done with our setup detailed in Section III Experimental Setup.

Another similar limitation is the constraint on the sample rate, maximum (suggested) sample rate of 56 MHz for the B210. For the PN signal, the bandwidth is related to the chip rate of the signal, which is in turn constrained by multiples of $\Delta t = \frac{1}{f_c}$, in which f_c is the chip rate. Similarly, in the Direct pulse case bandwidth is determined by the pulse duration which has the same constraint. In our case, the desired bandwidth is 40 MHz for an intermediate signal which is only obtainable if the PN signal is critically sampled with a sample rate of 40 MHz. In order to hold the sample rate constant across the waveform at 50 MHz, the obtainable chip rate for the PN signal is 16.7 MHz, leading to a bandwidth of 33.4 MHz.

Finally, the USRPs' front end filters introduce a transient response to the beginning of each of the signals resulting in a sweep-in of power each time the retuning process occurs. The envelope of the power sweep can be seen in Fig. 4.7 with the Zadoff-Chu stimulus.

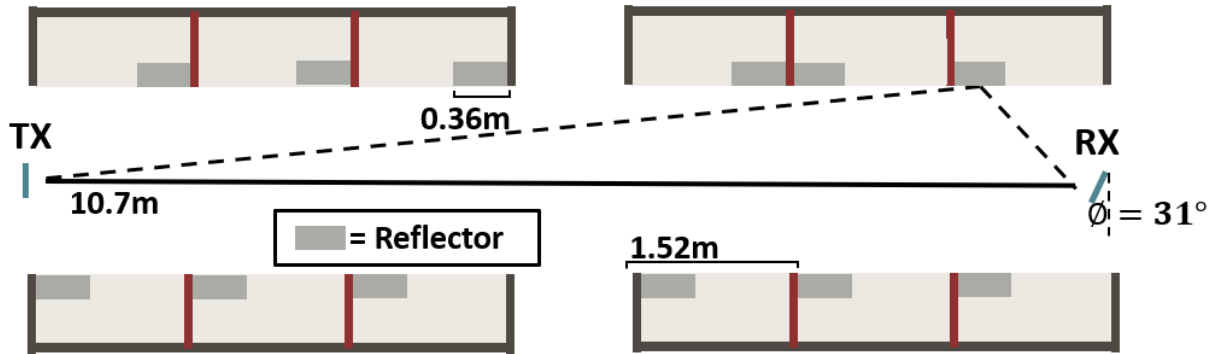


Figure 4.8: Visuals of Environment used to Collect Measurements with Metal Bin Reflectors

Knowledge of the existence of this transient response as well as the duration is important for the sounding performance especially considering the short length of the sounding signals. A path to mitigate this issue is to send several periods of an intermediate sweep before retuning to the next center frequency. Then, when calculating the PDP from the CIR block estimate, a section of the first and last estimate rows can be discarded to remove the distorted estimations taken during the transient ramp up and down.

4.5 Over-the-Air Measurements and Discussion

The environment to conduct the channel sounding measurements was chosen to be a short-range indoor, office environment; the specifics of which are shown in Fig. 4.8. In this space, there are several metal drawers lining the space between the transmitter and receive, offering several paths for the sounding signal to reach the receiver and thus lead to multiple MPCs in the environment to characterize. In this space, there are no moving reflectors or elements, making this environment conducive for measurement collection with our system which is constrained on a static channel. The transmitter and receiver are separated by a distance of

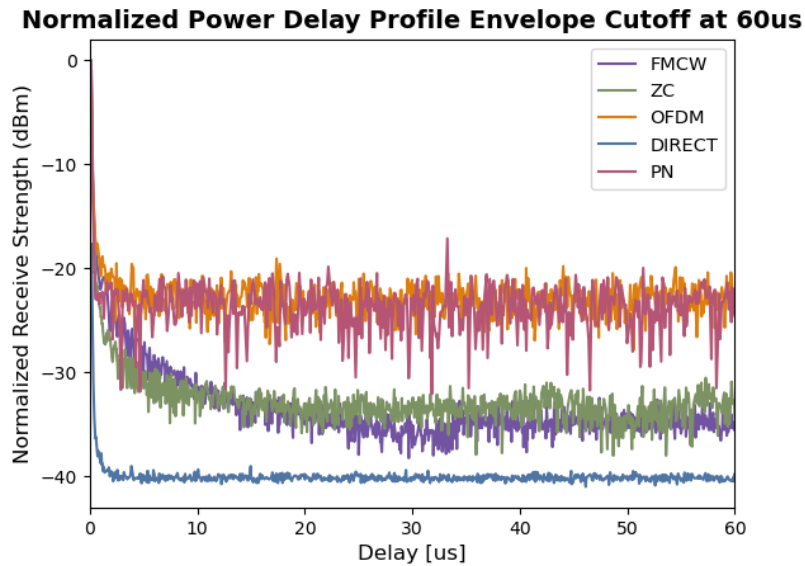


Figure 4.9: Envelope of Power Delay Profile with Each of the Sounding Waveforms

10.7 m. As illustrated in Fig. 4.8, the receive antenna is oriented towards a metal reflector to facilitate characterizing a strong MPC.

Fig. 4.9, shows the envelope of each of the PDPs obtained measuring the channel with each waveform cutoff at $60 \mu s$. In Fig. 4.9 the axis normalizes the highest PDP value among all waveforms to 0 dBm, but does not adjust the profiles scaling themselves. This view of the PDP can show deviations between the received power of each of the waveforms. Recall that each transmission waveform has the same aggregate energy and goes through appropriate scaling when making the channel impulse response blocks, meaning that it is expected for each waveform to be relatively close in received power. A noticeable deviation from this expectation is the direct pulse, whose peak on this normalized scale falls at -17.67 dBm. A potential explanation for this phenomenon occurring is that the high PAPR of the direct pulse could be outside the SDR achievable transmit amplitude range resulting in clipping. Also noteworthy in the left view of Fig. 4.9 is the spurious correlation peak in the PN case at $35 \mu s$, representing an indication from the PN measurements there is a MPC present

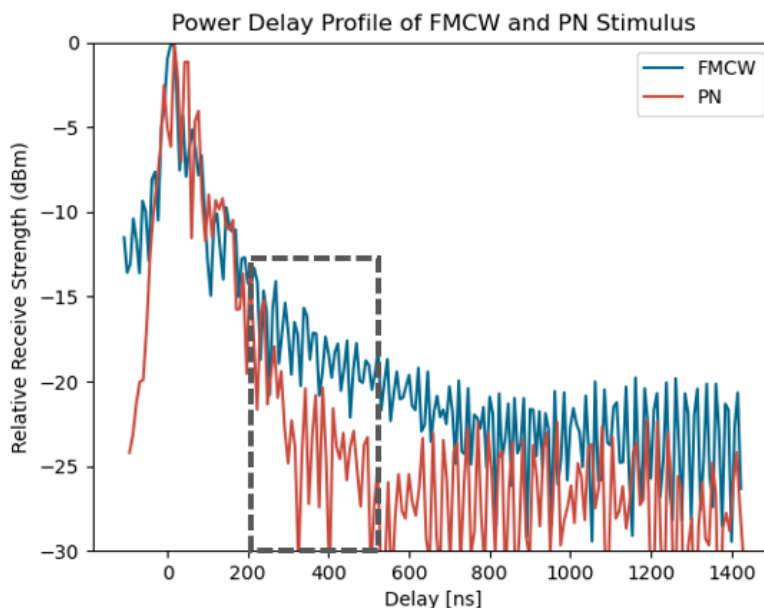


Figure 4.10: Power Delay Profile Obtained from FMCW and PN Stimulus Highlighting Sharp PN Decay

when there is not actually present in the physical environment. This behavior is indicative of a distortion in the correlation of the PN sequence, potentially due to the RF front end filters present in the B210 SDR. Table V. shows the peak received power relative to the other waveforms as well as the achieved dynamic range for each of the waveforms. As seen in Fig. 4.10 and Table V, the Zadoff-Chu and FMCW signals have the best achieved dynamic range performance, with the direct pulse and PN signals following, and the OFDM having the lowest achieved dynamic range.

Fig. 4.10. shows the overlaid power delay profile of the FMCW and PN waveforms clipped off at around $1.4\mu s$, with the receive strength floor being set to -30 dBm. Each of the PDPs seem to successfully characterize the same environment, while having the same general topology of the profiles. Specifically, each profile shows a few MPCs close delay to

the LOS component with strong received power. These components are presumably due to the reflector angled towards the receiver. From this figure, we can observe the PN signals decay more rapidly into the noise floor of the profile. Notably, despite the FMCW signal having the lower noise floor (larger achieved dynamic range), the PN signal's sharper decay makes it more distinguishable between sidelobes of the autocorrelation and MPCs at lower delay values.

4.5.1 Performance Analysis / Scenarios

Based off of the performance determined by the above metrics, we will consider different scenarios or environments in which it will make sense to use a certain waveform.

Scenario 1: Spectrum / Bandwidth Limited Environments

The Zadoff Chu, FMCW and OFDM signals are the best choice for sounding in environments where the spectrum is especially limited. PN and Direct pulse both have significant leakage into neighboring bands, which gives these waveforms a disadvantage when needing to share the spectrum with others. One such case where it is especially important to consider power leakage into other bands is in the Dynamic Spectrum access environments.

Scenario 2: Low Expected Maximum Excess Delay

In cases in which the maximum excess delay is expected to be low or when there is a substantial number of MPC are clustered near the LOS component, the PN or ZC sequences would make a good choice. While the PN sequence does not have as good dynamic range (see Table IV) as the FMCW signal, the FMCW signal has slower drop off, making it more challenging to distinguish between sidelobes and closer delay MPCs. The indoor environment

is an excellent example of having small excess delays, with indoor residential having delay spread on the order of 5-10 ns and indoor office having delay spread on the order of 10-100 ns [56].

Scenario 3: Time-Varying Channels

The case of sounding within time varying channels, such as V2V links, is not influenced by the choice of sounding waveform, but how fast the waveform is being used to excite the channel. As referenced in the Doppler Performance Metric Section 2.B.3, maximum unaliased doppler shift is dependent upon the rate at which the channel is being sampled. While not necessarily the PN sequence itself, but the PN sequence in the context of the PN sliding correlator could be less suitable for these cases as the time to take channel snapshots is proportional to the slide factor.

Scenario 4: Real-Time Channels Measurements

The OFDM sounding signal would make a good fit for sounding campaigns or measurement systems that are conducted within environments that require real-time channel measurements, such as Autonomous Factories. In such environments, the computational complexity of the post processing algorithm becomes a note of concern especially within the context of system processing capabilities. The frequency domain method, used for the OFDM sounding signal, relies on FFT operations that are less computationally complex than time domain correlation algorithms, which can reduce the speed of the system. However, in our sounding implementation a correlation was used for synchronization making the OFDM signal as computationally complex as the correlative method.

Scenario 5: Long Distance / Path Loss Measurements

In the cases of sounding outdoors for path loss measurements at long distances, the FMCW and Zadoff-Chu signal are excellent sounding waveform choices. From Fig. 4.9, the FMCW and Zadoff-Chu signals have the best achieved dynamic range even when normalizing aggregate energy amongst all of the waveforms. Further, these waveforms have the lowest PAPR, meaning that they would require less of a power back off than other waveforms to stay within the linear region of a power amplifier. These two factors lead the FMCW and Zadoff-Chu signals to have improved measurable path loss capabilities when compared to the other sounding waveforms.

4.6 Conclusions and Future Work

The purpose of this paper is to examine common channel sounding waveforms and gauge where their strengths and weakness lie in sounding the wireless channel. Particularly, our motivation is to understand appropriate selection of a sounding waveform based on environment characteristics. Analysis was performed based on looking at the properties of each waveform and their method of channel measurement in addition to performing measurements on the channel at 950 MHz. The goal for the over the air measurements was not necessarily to collect measurements of this channel, as there are not many new insights to be gain from this heavily researched band, but to compared the obtained results between the waveforms.

The results of comparison between waveforms from baseband waveform analysis and over-the-

Channel Sounding Waveform Performance

— FMCW — PN — ZC — OFDM — Direct

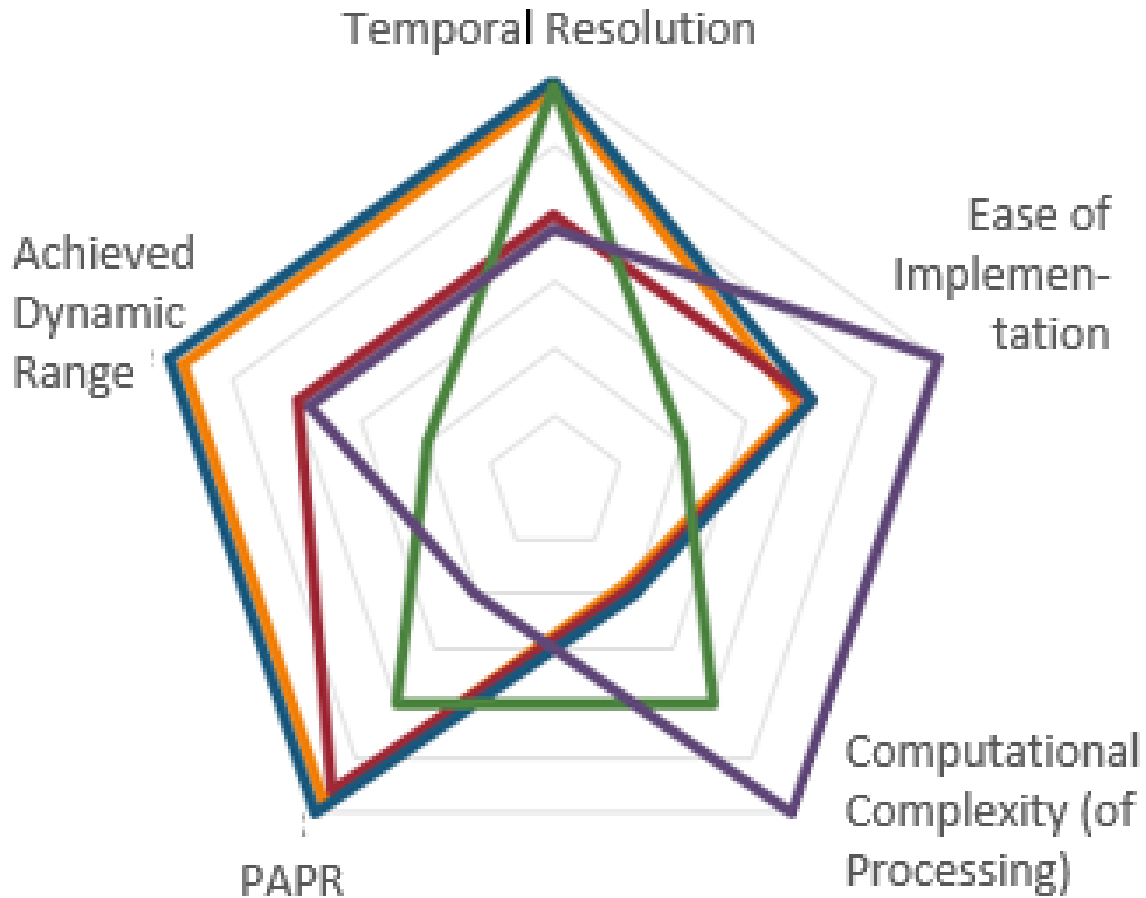


Figure 4.11: Waveform Channel Sounding Performance based on Specific Sounding Metrics - Spider Diagram

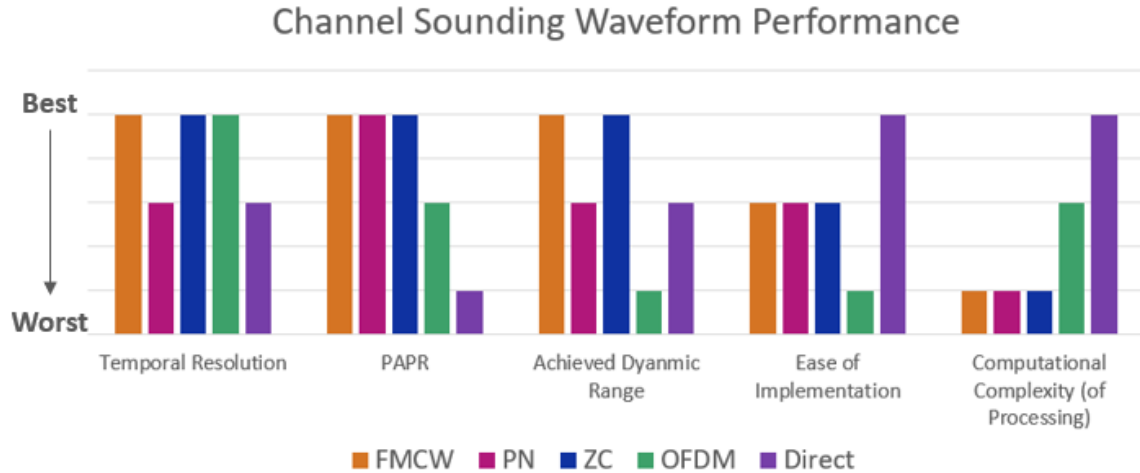


Figure 4.12: Waveform Channel Sounding Performance based on Specific Sounding Metrics - Multi-Category Bar Diagram

air performance metrics are summarized in Figs. 4.11 and 4.12 as well as in Table 4.3. The PAPR metric is based on desirability of the PAPR leading to a lower PAPR scoring higher, Doppler resolution and max excess delays are removed as they perform the same across each of the waveforms. From this figure we can see that the Zadoff-Chu and FMCW signal outperform the other waveforms in the categories of temporal resolution, achieved dynamic range, and PAPR, which are the categories that are related to the ability for the channel sounder to accurately characterize phenomenon in the channel. The Direct Pulse waveform performs the best in the remaining categories, ease of implementation and computational complexity (of processing algorithm) due to not having a processing algorithm.

The general performance results align with intuition, especially regarding each waveforms temporal and frequency resolution and PAPR performance. Further, based on Fig. 4.11 and overall performance explored, the waveforms can be ranked the following for general application with a SDR-based channel sounder: Zadoff-Chu, FMCW, PN, OFDM and Direct Pulse. While Zadoff-Chu and FMCW technically got the same groupings in the spider

Table 4.3: Summary of the Strengths, Challenges and Recommended Scenarios for each of the Sounding Waveforms Explored

Waveform	Strengths	Challenges	Scenarios
Zadoff-Chu	High Achieved Dynamic Range, Fine Temporal Resolution, Low PAPR, Sharp Autocorrelation Decay	Slightly Involved Post Processing – Time Complexity of Correlation	Spectrum / Bandwidth Limited Environments, Low Expected Maximum Excess Delay, Long Distance / Path Loss Measurements
FMCW	High Achieved Dynamic Range, Fine Temporal Resolution, Low PAPR	Slightly Involved Post Processing – Time Complexity of Correlation, Gradual Autocorrelation Delay	Spectrum / Bandwidth Limited Environments, Long Distance / Path Loss Measurements
PN	Decent Achieved Dynamic Range, Low PAPR, Sharp Autocorrelation Decay	Slightly Involved Post Processing – Time Complexity of Correlation, Spurious Correlation, Temporal Resolution	Low Expected Maximum Excess Delay, Implementation on a Sliding Correlator
OFDM	Fine Temporal Resolution, Frequency Response Method is Less Computationally Intense	High PAPR, Lower Achieved Dynamic Range	Spectrum / Bandwidth Limited Environments, Real - Time Channel Measurements
Direct Pulse	Minimal Processing Efforts	High PAPR, Temporal Resolution	Real - Time Channel Measurements

diagram, Zadoff-Chu slightly outperforms the FMCW signal, especially when considering the immediate drop of into the noise floor of the correlation of the Zadoff-Chu Signal. The PN signal is ranked higher than the OFDM signal for general application, even with the presence of the spurious correlation peak, due to improved PAPR and better achieved dynamic range. Lastly, the Direct Pulse was deemed the worst performance on the SDR platform since it had a significant drop in received power.

The determined ranking could be adjusted based off of looking outside of just utilizing SDRs. For example, the use of the PN sequence in a sliding correlator is easily implemented with shift registers and reducing cost with the ADC sampling rates. Also, the advantages of immediate acquisition of the CIR from the Direct Pulse can be better exploited with higher end DACs or specific pulsing circuits with the capable associated RF conditioning.

In addition to discussing the performance of the channel sounding waveforms, we proposed a lightweight channel sounding architecture that could be used to sound a variety of channels, using cheap transmitter equipment. The setup described can accommodate various sounding waveforms via playback files, intermediate frequency ranges from 70 MHz to 6 GHz, flexible bandwidth configuration, and can even be adjusted to accommodate other USRPs that have different RF constraints. While this system does not utilize low-cost SDRs for the receiver, the transceiver archetype can be modified to utilizing a Ettus USRP SDR at the receiver, replacing the IQ Recorder. In this setup, GNU Radio could be used for the USRP to record the received data into a file, but there would need to be a handshake between the transmit and receive devices to retune to the same frequencies at the same time. In the future, we plan on leveraging the channel sounding architecture described to sound mmW frequency bands to sound more meaningful channel environments.

Chapter 5

D-Band Path Loss Measurements

5.1 Abstract

Moving toward 6G involves accommodating for new data rate-intensive applications, which is challenging given current spectrum allocations. Thus, there is interest in incorporating use of higher frequencies bands, such as D-Band, to help support these applications. A crucial step before establishing a communications system is characterizing the wireless channel through channel sounding measurements. Many challenges exist in the implementation of sub-THz channel sounders, such as requiring operation across a wide bandwidth and needing to store and process large quantities of data. In this paper, we propose a flexible channel sounding architecture that is capable of measuring across D-Band with a configurable characterization bandwidth and dynamic selection of channel sounding waveform. Our overall contributions are summarized as follows: (1) detailed full system D-Band Channel sounder design, including hardware architecture and post-processing techniques, and (2) preliminary path loss measurement collected across 120-130 GHz at distances of 3 cm, 13 cm, and 36 cm.

5.2 Motivation

The transition from 5G to 6G technologies facilitates the exploration of new data rate-intensive applications. Some 6G use cases that require large data rates are holographic technology, extended reality, and tactile/haptic communications [76]. For example, displaying a holographic visual of a $6' \times 20''$ human in $4'' \times 4''$ tiles would require a data rate of 4.32 Tb/s [51]. Current spectrum allocations supported by 5G standards are not feasible for supporting these high data rate applications, and thus sub-terahertz (sub-THz) communication is one of several bands being considered to address the spectrum shortage [13]. One such sub-THz band that is being investigated for 6G is D-Band spanning from 110 to 170 GHz. Specific bands of interest within D-band have been identified, including 141-148.5 GHz, 151.5-164 GHz, and 167-174.8 GHz for fixed and mobile allocations [1]. However, [4] identifies the entirety of D-Band within a suitable spectral window according to the estimated path loss.

Utilizing sub-THz bands for communications introduces new challenges from propagation phenomena that are exacerbated with these higher frequencies. One challenge is substantially increased free space path loss observed at THz frequency, limiting the achieved distance for an omnidirectional communications link [38]. Surfaces considered smooth at lower frequencies also now introduce scattering losses from the short wavelength at sub-THz frequencies relative to the dimension of surface variations [39]. Molecular absorption is another challenge, introducing additional losses and contributing molecular absorption noise [35]. Sub-THz frequencies are susceptible to absorption from water vapor particles in the air, making signals more susceptible to weather fluctuations [11]. To overcome severe losses, communication systems employing sub-THz frequencies employ high-gain, narrow-beamwidth antenna architectures. However, there are some advantages of having highly directional communication links. The authors of [67] point out that THz propagation is resilient to undesirable effects such as diffraction, eavesdropping, and inter-antenna interference.

An important step before establishing a communications link is to have a thorough understanding of these propagation characteristics to gauge system operational constraints. Common channel sounder types aimed at characterization of THz channel are THz Time Domain Spectroscopy (THz-TDS), THz Time Domain Correlation (THz-TDC), and Vector Network Analyzer (VNA) approaches [31]. In the THz-TDS approach, a femtosecond laser, beam splitter, and THz emitter are used to radiate a short pulse with a THz wide bandwidth into the environment for direct channel characterization [34]. This method is able to achieve wideband measurements with extremely fast acquisition times, but is limited by transmission distance and peak-to-average power ratio, often leading to use in characterization of atmospheric and scattering affects [31]. The THz-TDC operates by transmission of a spread signal whose autocorrelation function resembles the Dirac Delta function and, upon pulse decompression, the channel is estimated [34]. This method is able to collect real-time measurements needed for time-varying channel characterization, but can be limited in bandwidth [53]. The frequency domain VNA approach measures the scattering parameter of the wireless channel as a Device Under Test (DUT) at incrementing carrier waves with the use of frequency extenders in THz channel sounding applications [34]. VNA approaches are able to measure a wide frequency band, but are limited to a direct connection between TX and RX and long measurement collection durations.

Creating accurate statistical channel models for sub-THz remains an open challenge due to requiring large amounts of channel measurement data [4]. However, there exists several measurement campaigns conducted to characterize propagation characteristics at sub-THz, including path loss, penetration loss, and foliage loss. Path loss measurements at 140 GHz were collected in [75] and fitted to the Close-In (CI) and Floating Intercept (FI) models. Also detailed in [75] is additional losses due to foliage for outdoor transmissions. In [68], two frequencies are considered, namely 158 GHz and 300 GHz, to make comparisons between

D band and H/J bands. With this analysis, a multi-frequency alpha-beta-gamma (ABG) model is considered in addition to the single frequency models, CI and FI. Several THz-TDC channel sounding systems have focused sounding 140 GHz for D-Band [31], leaving the 120-130 GHz range less investigated. Penetration loss and resulting delays from common indoor materials (plastic, paper, glass) at varying thickness levels were characterized in [44]. The authors of [14] compared models of path loss measurements of indoor links at 30 GHz, 140 GHz, and 300 GHz and determined that multi-frequency models were more stable than single-frequency models. In one study, D-Band (130 GHz) was deemed feasible for hop lengths of 40m-1km with LOS transmission [36]. Rain and atmospheric attenuation are included in these link budgets, using models from measurement collection.

The characterization of channel effects across varying frequencies has significant implications on the physical layer waveform design for a cellular generation. In 5G, specifications are separated based on carrier frequency with ranges defined as FR1 (below 6 GHz) and FR2 (23-32 GHz) [18]. Waveform construction varies slightly between FR1 and FR2, for example with FR1 having allotted 15 kHz, 30 kHz, and 60 kHz subcarrier spacing and FR2 having 60 kHz and 120 kHz subcarrier spacing [25]. These variations in Physical Layer design stem, in part, from known differences in propagation environment from moving to a higher frequency. Channel sounding efforts that characterize a wide frequency band, like in [83],[84], are crucial for the development of 6G physical layer design.

Channel characterization across several frequency bands is not only relevant to the PHY layer, but also to the MAC layer scheduling algorithms. Several studies have investigated scheduling and resource allocation (SRA) algorithms using channel state information (CSI) to maximize spectral efficiency [69],[81]. However, having perfect CSI can be an unrealistic assumption motivating the authors of [2] to investigate joint SRA using imperfect channels state information. In this study, the performance of imperfect CSI algorithms were com-

pared with algorithms with perfect CSI and no instantaneous CSI. Despite the imperfect CSI algorithms not performing as well as the perfect CSI case, algorithms with imperfect CSI performed substantially better than cases without any instantaneous CSI. In massive-MIMO (mMIMO) cases, CSI is necessary for both resource allocation and beamforming, but gauging the channel with CSI measurements from each antenna leads to significant overhead [17]. SRA efficiency and mMIMO overhead reduction motivate the ability to appropriately leverage CSI corresponding to a specific subband to multiple subbands.

There are two main contributions of our work summarized as follows: (1) a detailed full system THz-TDC D-Band channel sounder architecture design and implementation and (2) path loss measurements across different distances and frequencies within D-Band. In contribution (1), we describe the D-Band channel sounding architecture developed equipped with frequency retuning and dynamic channel sounding waveform selection. In-depth details of the system components including RF front end processing, channel sounding packet structure, Field-Programmable Gate Array (FPGA) programming, software to coordinate transmissions, and post processing algorithms. In contribution (2), we provide path loss measurements various distances and frequencies using the realized sounding architecture. Indoor measurements collected at distances of 3 cm, 13 cm, and 36 cm and frequencies across 120 GHz - 130 GHz in 184.32 MHz increments. These contributions add to a ever-growing body of work to collect sub-THz channel measurements needed to create predictive models. The structure of the rest of this paper is as follows: Section 5.3 describes the full D-Band channel sounding system architecture, Section 5.4 details the collected path loss measurements across varying distances and frequencies, and Section 5.5 offers conclusions drawn from our work as well as potential future research directions.

5.3 Wideband Channel Sounding System Architecture

In this section, we discuss the full composition of the channel sounding architecture, which has the capabilities of sweeping across any configurable range(s) within D-Band with a dynamic channel sounding waveform selection. For the purposes of this work, we swept 120 - 130 GHz. This architecture is able to achieve wideband channel characterization by re-tuning the center frequency after every channel packet transmission. The general system architecture is detailed in Fig. 5.1 and is composed of analog RF conditioning and software processing for transmission coordination and post-processing for path loss measurement extraction. On the transmit side, an FPGA operates as the Intermediate Frequency (IF) input into the sub-THz hardware architecture by generating channel sounding packet at a clock rate of 500 MHz. The received signal gets converted down to IF and recorded for post processing.

5.3.1 Hardware Architecture: RF Front End

The hardware architecture contains the RF front end elements that upconverts an input IF channel sounding signal to D-Band and downconverts the received signal back to IF. The elements of the hardware architecture can be seen in Fig. 5.1, specifically from the IF stage on the transmit side to the IF stage on the receive side. The transmit mixing stage to upconvert the IF signal to D-Band is driven by a local oscillator (LO) that is composed of a frequency synthesizer [22] and active frequency 12x multiplier [21] to reach D-Band frequency ranges. Although the frequency synthesizer is capable of generating frequencies anywhere between 0.2-20 GHz with a resolution of 0.1 Hz, we only considered the range of 10-11.67 GHz to achieve the desired range of 120-130 GHz with the active frequency multiplier. After the mixing stage, the signal goes through a D-Band bandpass filter to remove images. The

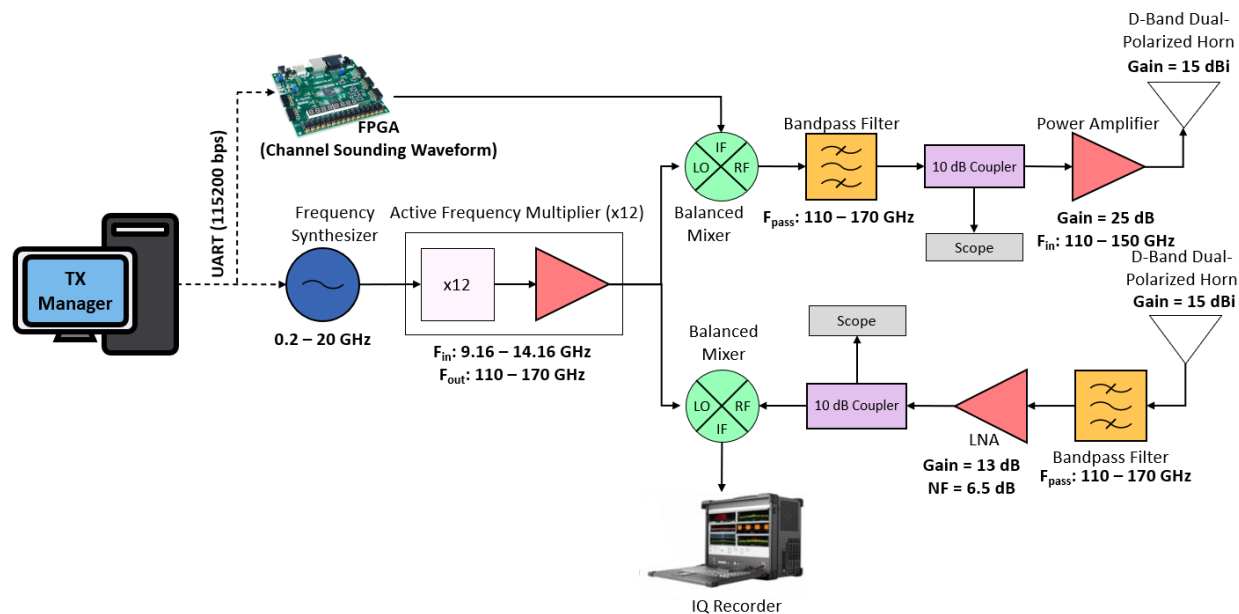


Figure 5.1: Full System Architecture

RF signal is then amplified with an Power Amplifier [20] and radiated into the environment with a D-Band Dual-Polarized Horn antenna [23].

The analog receive chain resembles the transmit chain, with the exception of substituting a Low Noise Amplifier (LNA) [19] in place of the Power Amplifier to limit noise. The received signal is captured through the RX D-Band Dual-Polarized Horn antenna and passes through a D-Band bandpass filter to isolate the signal spectrum of interest. After going through the amplification stage with the LNA, the signal is brought back down to IF using an LO composed of a frequency synthesizer and active frequency multiplier. At this stage, the IF signal is recorded for post processing using an IQ Recorder (VitreK EON CSE123G2 Signal Recording System) [78], which is composed of a GaGe CSE123G2 12-bit Digitizer with sample rate up of 3 GS/s, Signal Recording Software (SpectraScopeRT), and 38.4 TB in RAID storage.

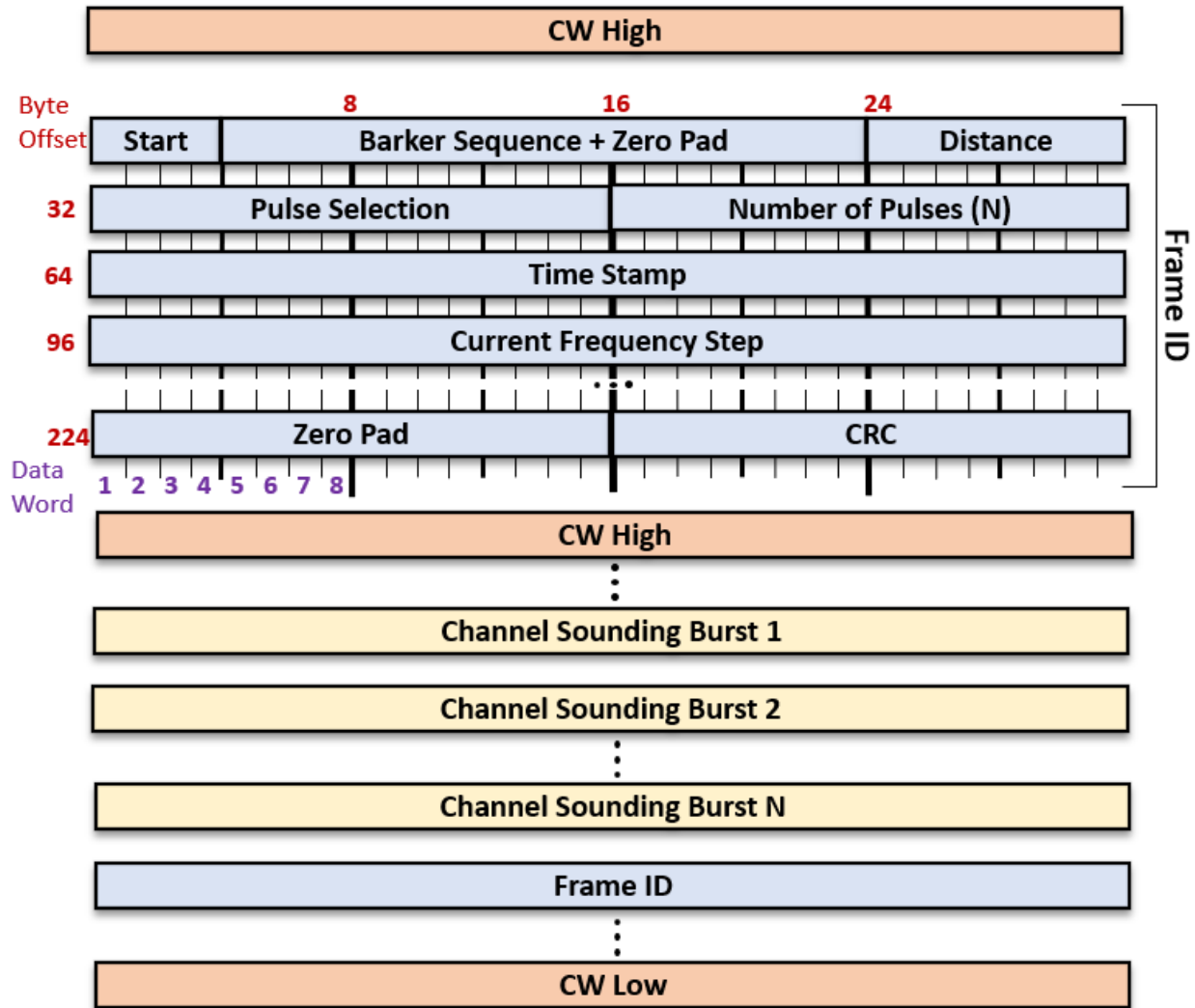


Figure 5.2: Frame ID Structure

5.3.2 Channel Sounding Packet Structure

A transmitted frame contains a stimulus of the channel used to characterize the path loss of a sub-band within the band of interest, mimicking [57]. The channel sounding waveforms within the packet are framed with a header and a trailer, which provides a low complexity method for synchronization, frequency offset detection, and communication of information relating to the transmission. Each of the individual channel sounding bursts can be selected

from a variety of baseband waveforms, alternating between emphasis on better time or frequency resolution [30]. The header is composed of an effective Continuous Wave (CW) signal at f_{high} , a two-tone FSK-modulated Frame ID with f_{high} to encode the 1s and f_{low} to encode the 0s, and shorter CW signal at f_{high} . Next in the packet is the channel sounding bursts with dynamic channel sounding waveform selection and number of burst repetitions, configured through the frame ID. The trailer consists of a CW at f_{low} and the FSK-modulated Frame ID, but with f_{low} to encode the 1s and f_{high} to encode the 0s.

The modulated Frame ID serves the purpose of conveying pertinent information regarding the packet transmission. The breakdown of the Frame ID, including the specific information at specific bit values, is shown in Fig. 5.2. Note that each information bit is repeated eight times at the 184.32 MHz sample rate to ease acquisition. Thus, the data word 0 is eight consecutive 0 bits and the data word 1 is eight consecutive 1 bits. The Frame ID contains 256 information bits, each repeated eight times to form a total length of 2048 bits = 256 words. In the subsequent subsection, we will break down each of the Frame ID fields with what information about the transmission they convey.

Start Indicator (Words 1-4)

The first four words of the Frame ID are all 0 to represent the start of the Frame ID. In the header, these data bits are modulated to f_{low} to distinguish from the CW High tone. For the trailer, these data bits are modulated to f_{high} to distinguish from the CW Low tone.

Barker-13 Sequences (Words 5-19)

Following the Start Indicator, are data words representing the Barker-13 sequence. The Barker-13 sequence has strong autocorrelation properties that assists in time synchronization,

if necessary.

Environmental Characteristics (Words 25-32)

The next eight data words are used to document any environmental characteristics relevant to the location and/or measurement setup.

Pulse Selection (Words 33-48)

The pulse selection field in the packet facilitates the ability for dynamic selection of channel sounding waveform in the packet. The FPGA that generates the packet waveform has a table/array of (Read-Only Memory) ROM addresses corresponding to memory locations of samples of various sounding waveforms. The value of this field corresponds to the index that designates which memory location the FPGA looks at to read samples for the sounding waveform. More details on the implementation of this on the FPGA is provided in Section [5.3.4](#), FPGA Mechanics.

Number of Pulses (Words 49-64)

The number of pulses field represents the number of repetitions of the selected channel sounding waveform within the packet. These data words get passed to the FPGA for dynamically setting the repetitions of the channels sounding burst as detailed in Section [5.3.4](#), FPGA Mechanics.

Time Stamp (Words 65-96)

The time stamp field represents a count in seconds since January 1st, 2024. With 32 data word for this field, approximately 139 years can be represented.

Current Frequency Step (Words 97-128)

The purpose of the current frequency step field is to document the center frequency the packet was transmitted over. This field is determined by representing the center frequency in units of kHz in binary. With 32 bits allocated to this field, frequencies within the range 0 - 4.29 THz can be represented, with 1 kHz resolution.

Cyclic Redundancy Check (Words 241-256)

A 16-word Cyclic Redundancy Check (CRC) is added to the frame ID for the purposes of error detection. The CRC is calculated in this paper by using the CRC16-CCITT polynomial [6].

5.3.3 Transmission Manager

The transmission (TX) manager is responsible for the coordination of continuously sending a channel sounding packet on the appropriate sub-band through interfacing with the FPGA and frequency synthesizer. Fig. 5.3 shows the block diagram for the TX manager created using Python and Fig. 5.4 illustrates communications between devices. The class will first accept user input to initialize state variables that will direct the transmission run. For instance, the user can control the start frequency, total sweep bandwidth, channel sounding waveform, and repetitions of the channel sounding waveform. Next, the TX manager will

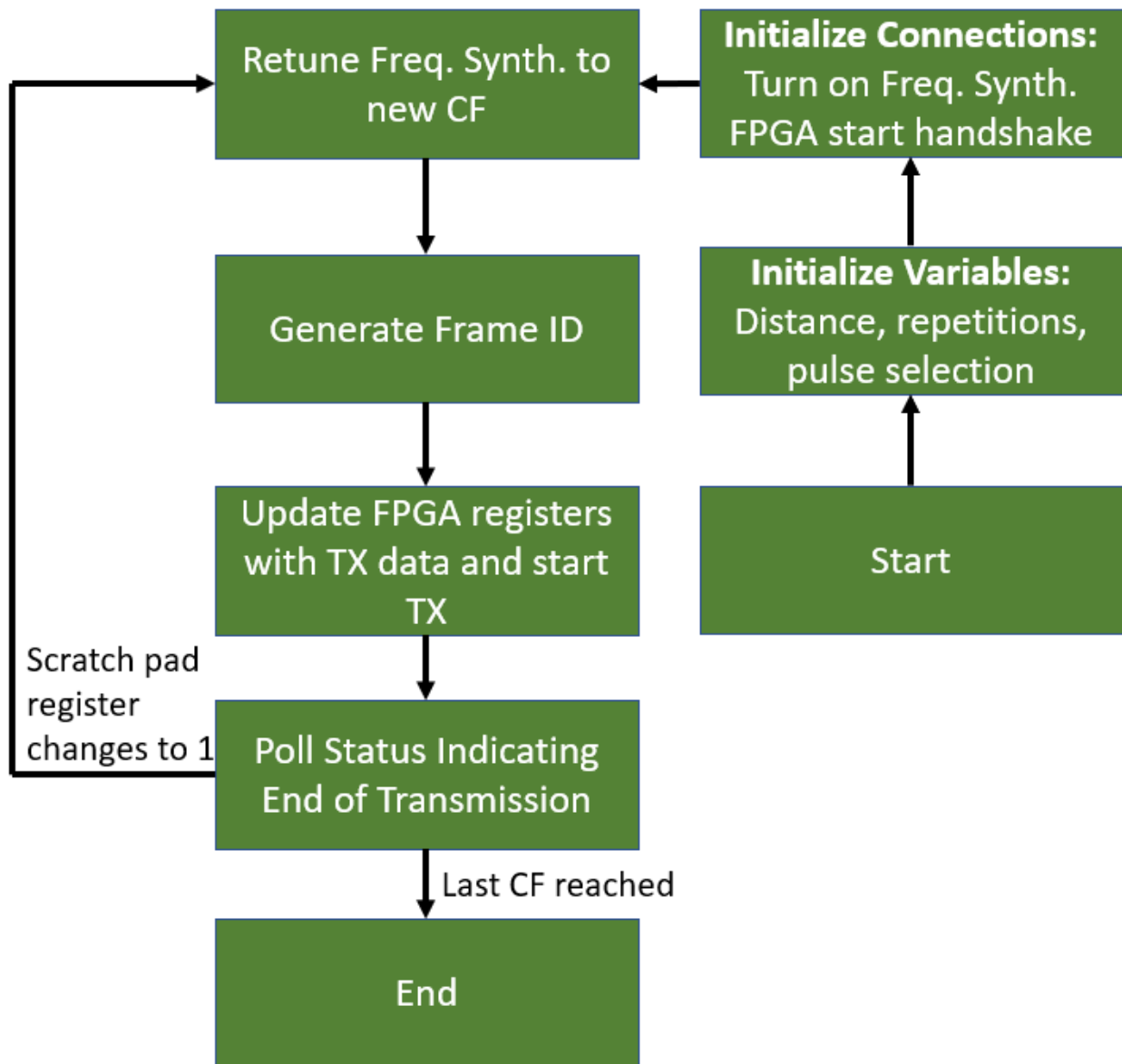


Figure 5.3: TX Manager Block Diagram

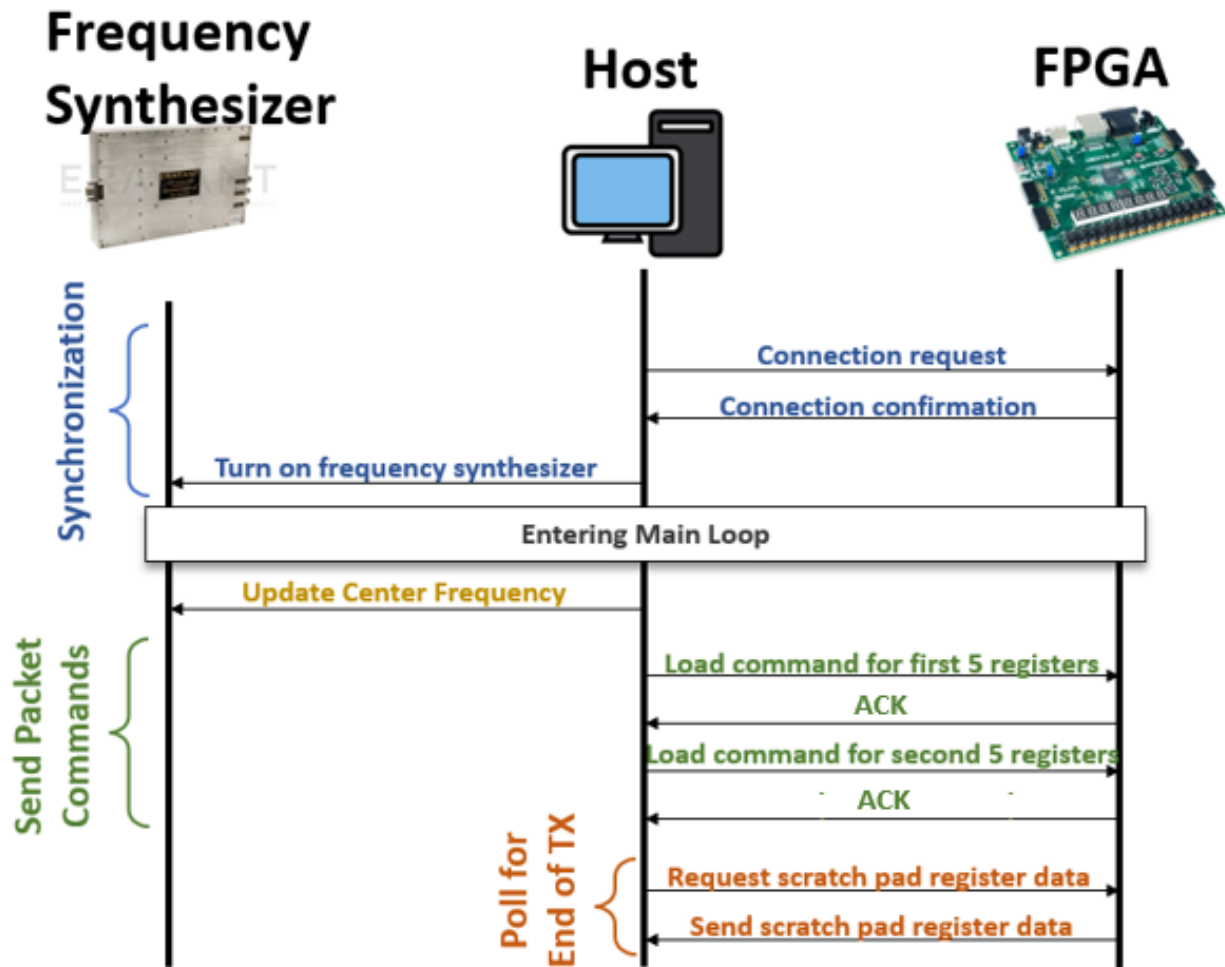


Figure 5.4: TX manager communications between host machine, frequency synthesizer, and FPGA

establish a connection the FPGA over UART by sending a connection request message and proceeding upon a received confirmation message. The last initialization step is turning the frequency synthesizer on using the synthesizer's UART command message protocol. Upon establishing hardware connections, the transmission manager will enter a loop that will continuously repeat the transmission process until the last center frequency is reached.

Upon reading in the start center frequency, the TX manager retunes the frequency synthesizer to the appropriate starting frequency by sending a UART request. After successful

retuning of the synthesizers to the new sub-band, a Frame ID is generated according to the specifications detailed under Frame ID within Section 5.3.2. The generation of this Frame ID will depend on initialization elements like current frequency and distance. The TX manager will send commands over UART to the FPGA that load registers with relevant transmission information including the generated Frame ID, pulse selection, and number of pulses. The loading register commands are split into two separate commands to the FPGA, where after the second is sent, the FPGA starts the transmission by setting a control register. The transmission manager continuously polls a scratch pad register on the FPGA that will switch when the transmission is over. Once the manager gets the message that the transmission of a packet is over, it will calculate the next center frequency. This would mark the end of one transmission run, as the transmission manager would loop back to retuning each of the frequency synthesizers to the new center frequencies.

5.3.4 FPGA Mechanics

The channel sounder was implemented on a Zynq UltraScale+ RFSoc ZCU111 Evaluation Kit, which features eight 12-bit 4.096 GSPS ADCs and eight 14-bit 6.554 GSPS DACs as a rapid hardware prototyping platform. There are three main components to the FPGA implementation: (1) an FSK modulator, (2) the channel sounding signal playback file reader, and (3) a state machine to control the transmission sequence. Modulation of the FSK signal is accomplished by incrementing or decrementing a 10-bit phase word based on the current bit in the channel sounding packet, where a ‘1’ corresponds to an increment and a ‘0’ corresponds to a decrement that occurs each clock cycle for the symbol duration. This instantaneous phase word is then taken as an address for the I/Q sample look-up table to provide 14-bit samples to the DAC (in each of I and Q).

The playback file reader is even more straightforward; when it is time to begin reading out the channel sounding signal(s), the FPGA is configured to sequentially read out the samples from a read-only memory (ROM) that is initialized when the design is synthesized. There are several different playback files stored in a ROM to choose from, and this information is passed to the FPGA as the “pulse selection” parameter. Additionally, the “number of pulses” parameter is also considered to determine how many times the selected ROM is to be repeated.

The state machine was constructed to monitor the FPGA registers to determine whether a new FSK packet is available for transmission, then enter the FSK modulation phase before reading out the channel sounding signal from the playback file ROM for a set number of repetitions. Transmission concludes with the inverted FSK bits and a CW low tone. To conclude the transmission, the state machine requires the control register bit to be de-asserted before allowing a new transmission to begin.

5.3.5 Receiver Post Processing

The received 500 MHz IF channel sounding signal is captured using the IQ Recorder, which is the terminating stage of the receive chain. The IQ Recorder collects the observed IQ samples into a raw data file that contains the received IF signal measured at all center frequency within the 120-130 GHz sweep. Using Python, the recorded received samples are digitally converted to complex baseband with digital filtering, and downconverter and decimated to the FPGA clock rate (184.32 MHz). The complex baseband samples are correlated with the selected channel sounding waveform for time alignment and path loss measurements. An example of the output at the correlation stage is shown in Fig. 5.5. The different packet elements can be extracted based on knowledge of the start index of

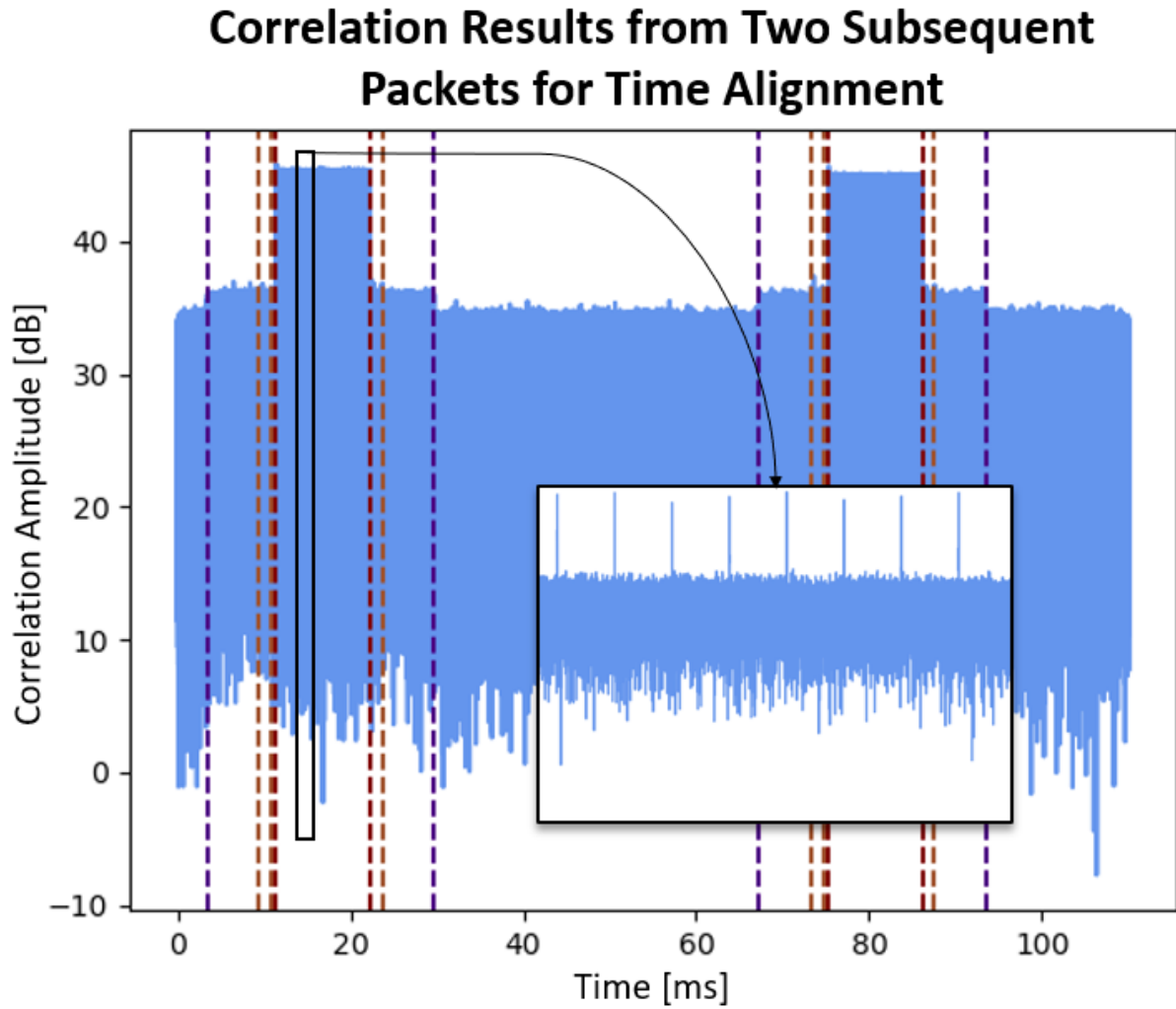


Figure 5.5: Two received packets correlated with transmitted pulse to illustrate time alignment for packet decomposition and analysis

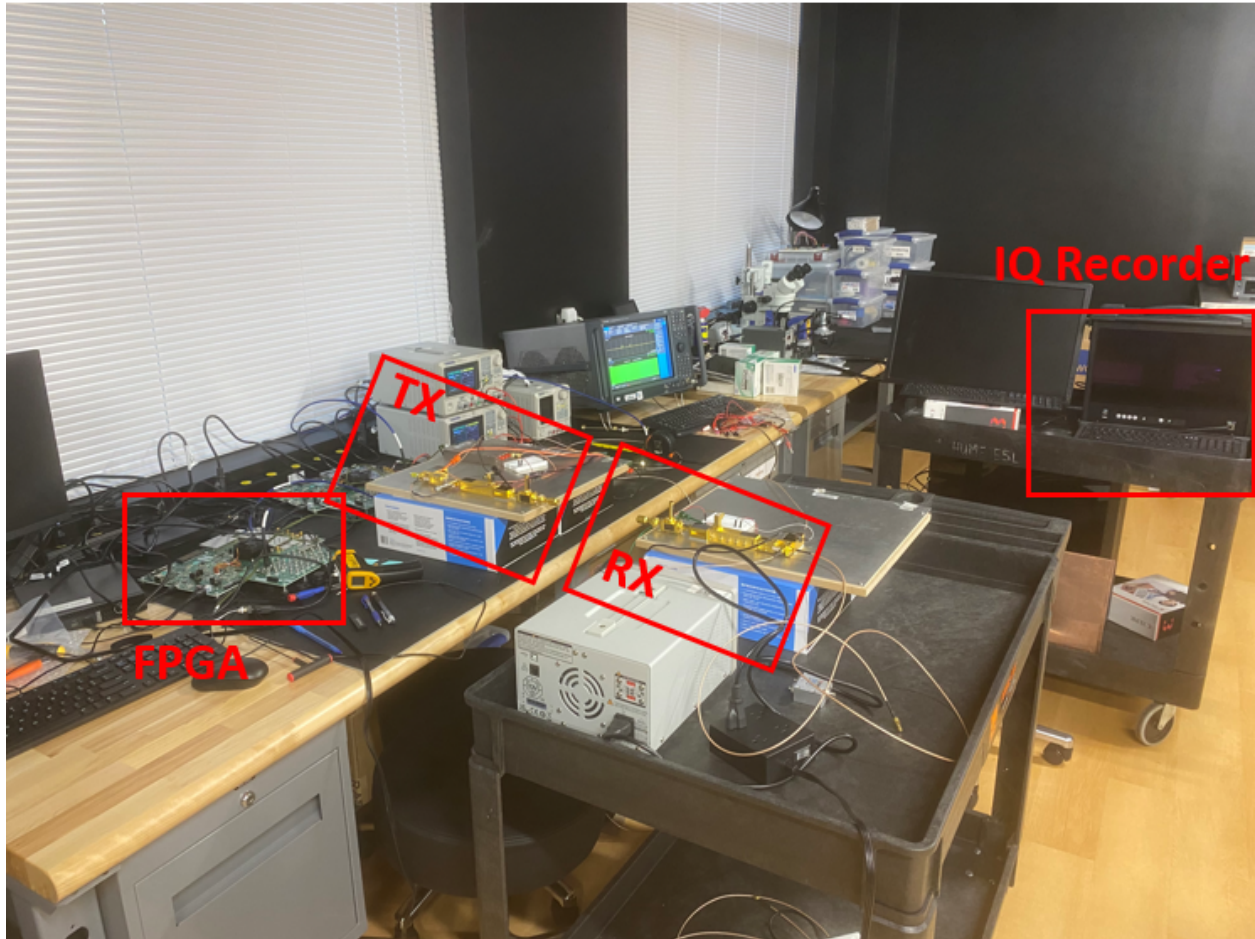


Figure 5.6: Hardware Setup

the channel sounding waveforms and, of course, knowledge of the packet structure. Upon isolating each of the packet elements, the FSK frame ID section is demodulated and average peak correlation power information is extracted and stored within an Excel file entry. The process of isolating packet elements and recording information pertaining to path loss occurs until each detectable packet has been processed.

5.4 Preliminary Measurement Collection

5.4.1 Experimental Setup

In our setup, we collect path loss measurements by determining the additional loss with reference to a direct waveguide connection. We accomplish this by comparing the observed average peak correlation power at a particular distance to that of the system connected by waveguide. Fig. 5.6. is a picture of the hardware system with boxes labeling relevant subsystems, including the transmitter sub-THz front end, receiver sub-THz front end, transmitter FPGA, and receiver IQ Recorder. The transmitter is stationed at a fixed point on a laboratory desk and the receiver is positioned on a cart to test at various distances. The measurement collection environment is an indoor, laboratory environment at a very short range.

5.4.2 Link Budget of System

Table 5.1: Link Budget of Example -13.2 dBm Sinusoidal

Component	Power In	Gain
Transmitter		
Mixer	-13.2 dBm	-13 dB
Attenuator	-26.2 dBm	-3 dB
Bandpass Filter	-29.2 dBm	-3 dB
Coupler	-32.2 dBm	-3 dB
Power Amplifier	-35.2 dBm	25 dB
Receiver		
Bandpass Filter	-10.2 dBm	-3 dB
LNA	-13.2 dBm	13 dB
Coupler	-0.8 dBm	-3 dB
Mixer	-3.2 dBm	-13 dB

Before collecting channel sounding measurements, a -13.2 dBm tone was propagated through

the sub-THz transceiver with waveguides connecting the transmitter and receiver. In our system, we are constrained to have a maximum TX IF power of -12 dBm motivated from the maximum power allowed into the IF port of the mixer. For this example the expected gain from going through each component of the system is highlighted in Table 5.1. From Table 5.1, the expected received power of the system is -16.2 dBm with waveguide connection and the measured received power was -23.3 dBm. Thus, about 7.1 dB of loss currently unaccounted for in the transceiver design, which could be explained from losses due to waveguide connections or insertion losses of the components.

5.4.3 Short Range Path Loss Measurements

Measurement collections are limited to less than 0.5 m between the transmit antenna and receive antenna due to the current hardware architecture. With this distance limitation, we have measured collected signal strength and path loss measurements at distances of 3 cm, 13 cm, and 36 cm. For measurements collected at each of the distances, the frequency range 120 - 130 GHz is measured by adjusting the center frequency of each channel sounding packet, starting at 120 GHz and incrementing by the bandwidth of the channel sounding bursts until the center frequency reaches 130 GHz. Fig. 5.7 shows the observed signal strength from each of the collections at distances of 3 cm, 13 cm, and 36 cm. In the 36 cm case, the channel sounding packets become undetectable at 125 GHz and thus no signal strength measurements are recorded past this point. Packets become undetectable when the signal power, even after de-spreading gain, cannot surpass the noise floor, in our case being close to -81 dBm.

Looking at the raw received signal strength data, without normalizing any system responses, provides insights into specific link performance areas relevant to the realized system. From

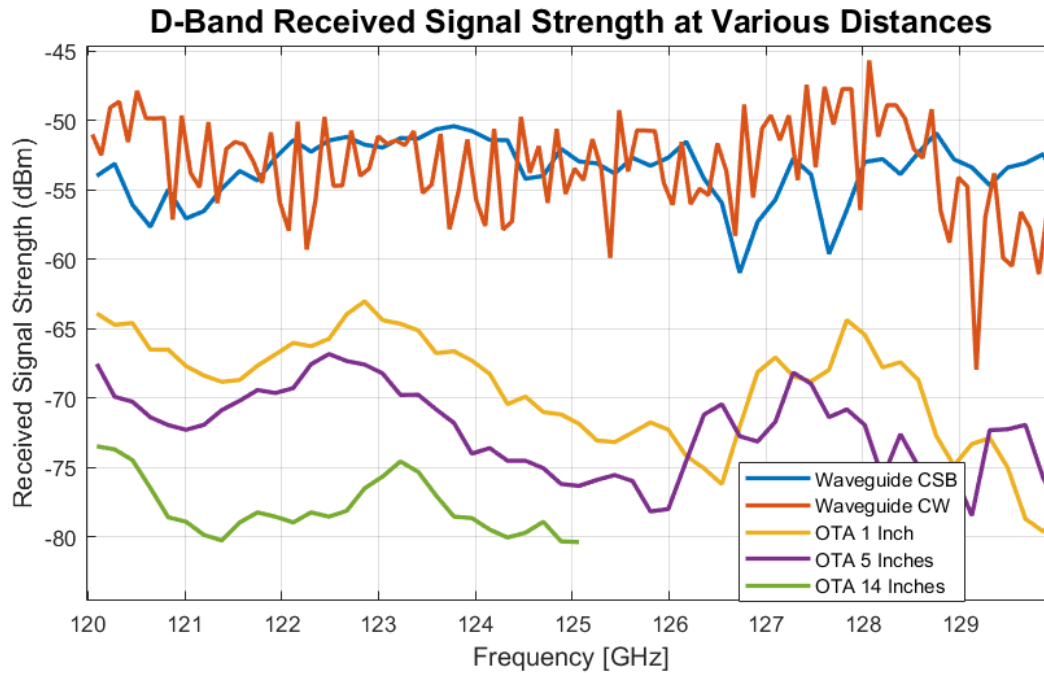


Figure 5.7: Received signal strength across D-Band frequencies and short range distances

Fig. 5.7, the frequency ranges 120-120.5 GHz, 122.5-123.5 GHz, and 127.5-128 GHz experienced the highest received signal strength. The frequency ranges 120.5-122 GHz, 126.5-127.5 GHz, and 128-129 GHz experienced the next highest received signal strength. Lastly, the frequency ranges 124-126.5 GHz and 129-130 GHz experienced the lowest received signal strength. Notably, we are able to categorize frequency ranges into bins of similar observed signal strength. Leveraging the knowledge of which bands behavior similarly within our system can allow us later to make conclusions about one band given real time information of another within a similar range.

Path loss measurements are determined from recording the signal strength experiences at these these varying distances relative to a waveguide strength measurement. The importance of normalizing to the waveguide measurements is that our signal strength measurements represent not only losses experienced from the channel, but also losses introduced from our sub-THz channel sounder. By subtracting the losses experienced at each frequency with

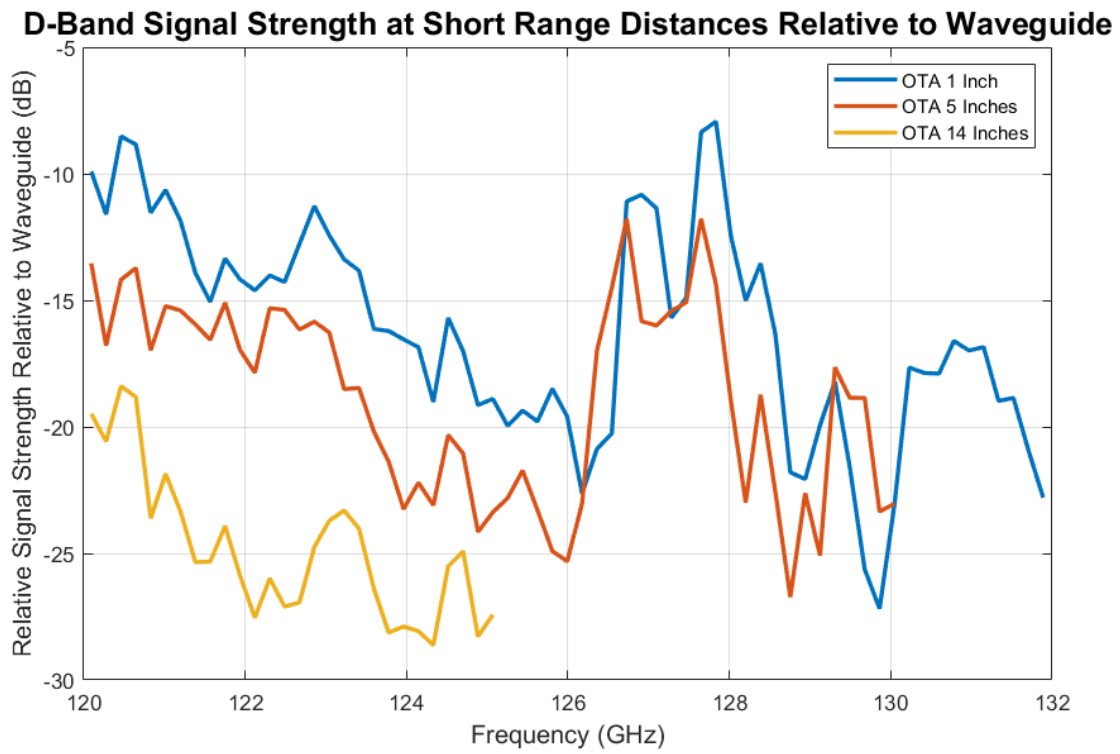


Figure 5.8: Received signal strength across D-Band frequencies and short range distances relative to waveguide measurements

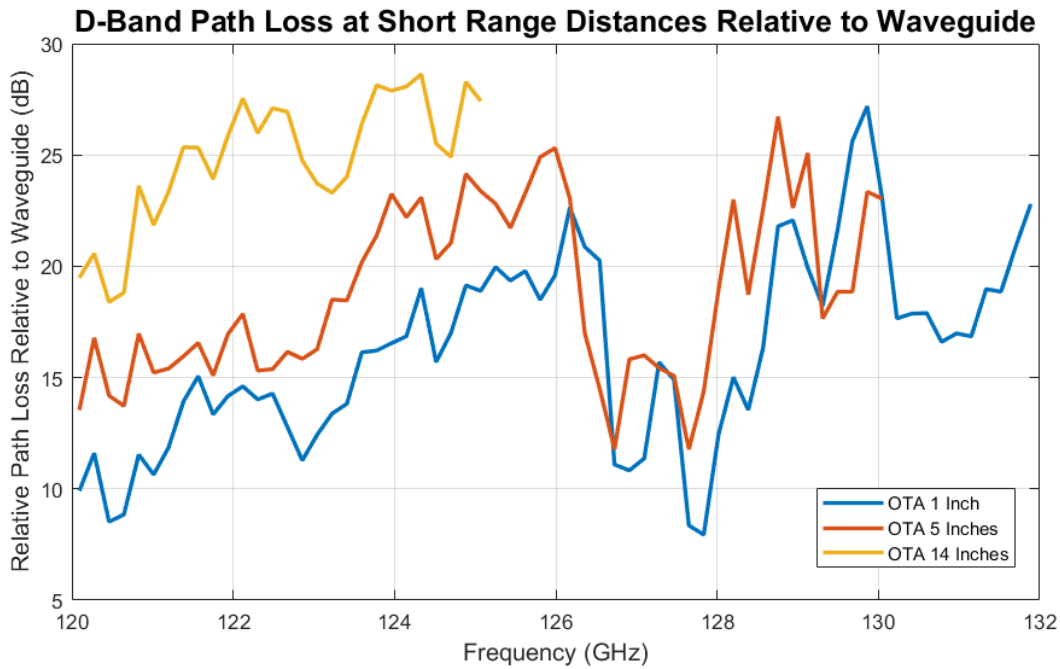


Figure 5.9: Path loss measurements from 120 - 130 GHz normalized to waveguide measurements

the waveguide connection, the losses due to the physical channel can be more accurately estimated. Fig. 5.9 illustrates the path loss experienced relative to waveguide measurements across the frequency sweep and at varying distances. From Fig. 5.9, there appears to be a favorable channel environment present across distance around 127 GHz due to the drop in path loss. Note that normalizing from the signal strength from the waveguides removes the dip in receive signal strength around 121 GHz for the path loss measurements introducing a more steadily increasing path loss as frequency increases (for the range of 120-126 GHz).

Also from Fig. 5.9, the increase in path loss between the 3 cm distance and the 13 cm distance is about 5 dB and the increase in path loss between the 3 cm distance and the 37 cm path is about 10 dB. The authors of [14] measured path loss across D-Band at different short range distances using a VNA channel sounder. With this setup, the measured approximately a 3 dB increase in path loss from 36 cm to 45 cm and an 10 dB loss from 36 cm to 66 cm.

While these results are at a slightly higher distance than our measurements, the results seem consistent in path loss differences across distance.

5.5 Conclusions and Future Work

In this paper, we detailed a D-Band channel sounding architecture capable of dynamic re-tuning, waveform selection, and pulse repetitions. With current post-processing architecture and hardware constraints, the system is capable of measuring path loss at distances up to 36 cm. Preliminary path loss measurements were collected to contribute growing effort for D-Band channel characterization as well as validate realized system architecture. Path loss measurements were collected at distances of 3 cm, 13 cm, and 36 cm with an increase in path loss of about 5 dB going from the 3 cm path to the 13 cm path and about a 12 dB increase going from the 3 cm path to the 36 cm path.

In the future, our group will focus on extending the distance capability to collect path loss measurements across 120-130 GHz at larger distances by incorporating an additional gain stage. Additional efforts will/can be placed in using the estimated CIR response to derive more channel parameters including delay spread, angle spread, and doppler spread. Other future directions include employing the realized channel sounding architecture in various environments to observe difference in channel behavior in difference scenarios.

Investigating path loss variation across different frequencies within D-Band would be useful information in defining 6G PHY layer standards. Additionally, observations regarding deviations between path loss observed at different frequencies could be useful in SRA algorithms. Specifically, in making conclusions about the CSI about one band given the CSI at another if these bands have similar path loss. Incorporation of frequency selective path loss could be beneficial in SRA algorithms to ease CSI transmission overhead or combine recent CSI from

other bands with memory of CSI. For example, outdated information is one of the drivers of having imperfect channel knowledge [73]. Incorporating knowledge of subcarriers that have similar path loss responses could facilitate keeping multiple carriers with more up-to-date information with new of one carrier coming in. In these cases, CSI for bands with similar expected path loss could be predicted as being the same, potentially increasing the accuracy of the channel estimates in real time.

Chapter 6

Conclusions

6.1 Discussion

Overall, the work contained within this thesis offers contributions to flexible channel sounding develop by offering two different system architectures that enable dynamic channel sounding. One of the architectures involves a low-cost SDR based approach and the other uses custom FPGA-based hardware with D-Band RF conditioning to measure sub-THz frequencies. While each approach differs in implementation, they both fundamentally centered in offering flexibility to a channel sounding measurement campaign. In both hardware systems, the user can specify what frequency range to transmit, including start frequency and full bandwidth, as well as the waveform that is being used to stimulate the channel. The main limitation with frequency band selection is that the selected range must be within the operational constraints of the hardware being used. However, for the low-cost SDR approach the achievable bandwidth goes from 56 MHz to just shy of 6 GHz, a substantial increase. For the D-Band channel sounder, the current achievable sounding bandwidth 40 GHz.

Benefits of utilizing a flexible channel sounder include (1) having the ability to sound more dynamic environments and (2) utilize the same channel sounder for different scenarios. In certain channel sounding environments, like operating within a Dynamic Spectrum Access environment, the allowable bandwidth and frequency band of operation may vary. With operating under dynamic conditions, it is helpful to have a channel sounder capable of flexi-

bility in adjusting these parameters. Also, there is a non-trivial amount of effort in designing a channel sounder. Thus, the second benefit of the flexible channel sounder is opportunity to use the same sounder in a variety of setting, with potentially different sounding needs. As detailed in Chapter 4, selection of channel sounding waveform impacts system performance and some sounding waveforms may perform more desirable in differing scenarios. For example, the PN signal has a sharp decay in autocorrelation function, but large frequency domain sidelobes. These characteristics make the PN signal not be the best choice in bandwidth limited/constrained environments but excellent for scenarios with short expected excess delay, such as the indoor environment. Allowing for flexible selection of sounding waveform, as well as band of operation, opens up potential use cases for the designed channel sounder.

The first architecture is geared to be more accessible by providing a channel sounding system that can be implemented with a low cost radio. Among other contributions, this accessibility can allow more students to engage with the field of channel sounding with a lower cost of entry. The low cost channel sounding transmitter design contains frequency retuning in order to aggregate to a larger bandwidth. In this first version of this SDR channel sounding transmitter, there was an additional polling delay for the transmission manager needed to check if the intermediate transmission had finished. In version two of the low-cost SDR channel sounding transmitter, GNU Radio, along with this additional delay were deprecated in favor of directly interfacing to the UHD Python library.

A complete low-cost SDR based channel sounder architecture was provided, using the updated, version 2 transmitter design. With this architecture it is possible to configure the start frequency, full bandwidth, step bandwidth, number of repetitions before a retune, and channel sounding waveform. This architecture was used to collect channel sounding measurements and graph the power delay profile of the channel for different channel sounding waveforms implemented on the low cost software radio: FMCW, Zadoff-Chu, OFDM, PN,

and Direct pulse. Each of these waveforms were normalized to the same bandwidth and the same aggregate energy. In this investigation, due to the high Peak to Average power ratio for the Direct pulse, it seemingly was not able to achieve the same aggregate energy as the other pulses with getting seemingly getting clipped. The Zadoff-Chu overall performed the best, offering a high dynamic range and a steeper autocorrelation drop off than the FMCW signal.

The transition from the low-cost SDR channel sounder to the implementation of the THz-TDC sounder using hardware capable of D-Band transmission inspired incorporation of many of the same flexibility features. A significant flexibility feature is the ability to artificially increase the instantaneous bandwidth to be limited by the operational frequency range of the hardware. Of the three THz sounding approach, THz-TDC, THz-TDS, and VNA, THz-TDS and VNA usually achieve higher bandwidths than THz-TDC. Thus, with the retuning adjustments, we will be able to reap the benefits of the THz-TDC sounder, fast measurement collection time and ability to collect data from a wider range, and overcome one of the identified drawbacks of a smaller bandwidth.

The D-Band channel sounder consists of a sub-THz RF conditioning, an FPGA for the IF source, and software processing to coordinate each transmission and process the received waveform. The sub-THz TX Hardware consists of the LO to convert the signal to D-Band with a frequency synthesizer and an active frequency multiple, as well as filtering and amplification before being emitted out of a D-Band Horn antenna. The RX Hardware is nearly identical, replacing a power amplifier for a low noise amplifier. The dynamically selected channel sounding bursts get framed by a header and trailer that consists of CW tones and an FSK-modulated frame ID. The frame ID contains information pertaining to a specific channel sounding run. The FPGA acts as the IF source, performing the FSK-modulation for the header and trailer and sending out the stored channel sounding waveform samples at an IF

frequency of 500 MHz. The transmission manager coordinates the details of the transmission by prompting the FPGA to start sending information on a specific center frequency with a specific sounding waveform and retunes the frequency synthesizer to the current center frequency with the UART connection. Finally, post processing is performed after digital downconversion from IF to baseband by correlating the received signal with the transmitted signal.

With the described D-Band channel sounding platform, short-range path loss measurements were collected in an indoor, laboratory environment. Measurements were collected at distances of 36 cm, 45 cm, and 66 cm. In order to attempt to accommodate for additional losses introduced to our system, potentially losses that were frequency dependent, the path loss measurements are reported relative to measurements collected with a waveguide connection. From the measurements, there was approximately a 3 dB increase in path loss from 36 cm to 45 cm and a 10 dB increase in path loss from 36 cm to 66 cm.

Initial validation of realized D-Band channel sounder contributes to the current body of channel measurements research as well as demonstrates the feasibility of using this system for future campaigns. Throughout characterization of the sub-THz channel is essential for creating accurate predictive channel models, and thus channel measurements from a variety of organizations with different channel sounder implementations is crucial for a holistic understanding of the channel. With this in my, our channel measurements can be used in conjugation with measurements from other universities and organizations, when appropriate, in the development of channel models for sub-THz indoor communications. Channel models can then be used to develop the constraints of an indoor sub-THz communications link, facilitating the ability to access more bandwidth. Not only did this work provide initial path loss measurements, but it demonstrates that the sub-THz channel sounder can be utilized in other scenarios given the flexibility of the sounder design.

6.2 Recommendations for Future Work

While the work contained within this thesis is primarily experimental in nature, several result generalizations can be made to pertain to other future work. The collected PDPs from Chapter 4 are relevant in comparing the performance of each of the channel sounding waveforms. The performance across several relevant metrics is then synthesized to make generalized recommendations of sounding waveform based on scenario. In Chapter 5, D-Band path loss measurements are collected from a LOS connection at varying short range distances. Sub-THz communications is most feasible with LOS connections and at a relatively short range, thus these measurements can be generalized and relevant to development communications under these constraints. However, the development of accurate channel model requires a large body of channel measurements of a variety of channel sounding scenarios, collected from a variety of organizations.

Detailed below are recommendations on future areas of development based off of the findings of the work presented in this thesis. Most of the topics presented here for further development involve expanding upon the D-Band channel sounder to characterize more meaningful channel environments.

- **Create a low-cost SDR channel sounder receiver that could operate in conjunction with the detailed low cost channel sounding transmitter.** A handshake would need to get introduced to the system to coordinate the frequency retuning of the transmitter.
 - Characterization and analysis could be performed regarding how fast this handshake between the SDR could take place, particularly in reference to the coherence time of the channel being sounded.

- **Integrate a dedicated pulsing device to more effectively wideband impulse without the limitations of the SDR.** With this additional hardware setup, the channel sounding performance can be compared to that achieved with the SDRs. Overall, a similar exploration of channel sounding performance can be carried out with opening up the constraint on implementation on the same SDR hardware.
- **Leverage the ability to select a different channel sounding waveform with the D-Band architecture and analyze any difference in performance.** With this setup, the performance of various channel sounding waveforms outside the software defined radio framework could be analyzed to see if there are any dramatic performance differences between hardware architectures.
- **Make enhancements to the D-Band RF Hardware to perform channel sounding measurements at D-Band with larger, more meaningful distances.** For example, incorporating higher gain TX/RX antennas would increase the dynamic range of the architecture, translating to the ability to transmit over a larger distance. However, this adjustment would require more directional antennas and potentially require stricter methods of aligning the antennas.
- **Place transmitter and receivers on set plates that can adjust in distance apart from each other to better align the directional antennas.** Additionally, have these plates be able to adjust the angle between the two for additional testing capabilities (angle of arrival).
- **Utilize two different frequency synthesizers for the D-Band architecture** (one for each TX and RX) and incorporate frequency offset processing to handle any frequency drift between the oscillators. Incorporation of an additional oscillator may be more practical and allow for longer TX/RX distances without need for excessively

long cabling.

- **Measure additional sub-THz phenomena including, but not limited to, delay spread, penetration loss, doppler spread, and angle of arrival.**
 - With this additional area of research, the assumption of a static environment could be removed to explore less controlled channels that vary with time (potentially outdoor channels).

Bibliography

- [1] TeraHertz technology (THz); Identification of frequency bands of interest for THz communication systems. Technical Report GR THz 002 V1.1.1, ETSI, March 2023. [Online]. Available: https://www.etsi.org/deliver/etsi_gr/THz/001_099/002/01.01.01_60/gr_THz002v010101p.pdf.

- [2] Rohit Aggarwal, Mohamad Assaad, C. Emre Koksal, and Philip Schniter. Joint Scheduling and Resource Allocation in the OFDMA Downlink: Utility Maximization Under Imperfect Channel-State Information. *IEEE Transactions on Signal Processing*, 59(11): 5589–5604, 2011. doi: 10.1109/TSP.2011.2162953.

- [3] Julian Ahrens, Lia Ahrens, Michael Zentarra, and Hans Dieter Schotten. Signal Restoration and Channel Estimation for Channel Sounding with SDRs. In *Mobile Communication - Technologies and Applications; 26th ITG-Symposium*, pages 1–6, 2022.

- [4] Ian F. Akyildiz, Chong Han, Zhifeng Hu, Shuai Nie, and Josep Miquel Jornet. Terahertz Band Communication: An Old Problem Revisited and Research Directions for the Next Decade. *IEEE Transactions on Communications*, 70(6):4250–4285, 2022. doi: 10.1109/TCOMM.2022.3171800.

- [5] Muhammad Sohaib Amjad, Gurjashan Singh Pannu, Agon Memedi, Muhammad Nabeel, Johannes Blobel, Fabian Missbrenner, and Falko Dressler. A Flexible Real-Time Software-based Multi-Band Channel Sounder. In *2020 IEEE 31st Annual International Symposium on Personal, Indoor and Mobile Radio Communications*, pages 1–6, 2020. doi: 10.1109/PIMRC48278.2020.9217369.

- [6] Anycrc. Anycrc: Flexible CRC calculation in Python. GitHub repository, 2024. Available at: <https://github.com/rzbrk/anycrc>.
- [7] C. Umit Bas, Vinod Kristem, Rui Wang, and Andreas F. Molisch. Real-Time Ultra-Wideband Channel Sounder Design for 3–18 GHz. *IEEE Transactions on Communications*, 67(4):2995–3008, 2019. doi: 10.1109/TCOMM.2018.2889487.
- [8] P. Bello. Characterization of Randomly Time-Variant Linear Channels. *IEEE Transactions on Communications Systems*, 11(4):360–393, 1963. doi: 10.1109/TCOM.1963.1088793.
- [9] Hervé Boeglen, Albekaye Traore, Manuel Milla Peinado, Romain Lefort, and Rodolphe Vauzelle. An SDR Based Channel Sounding Technique for Embedded Systems. In *2017 11th European Conference on Antennas and Propagation (EUCAP)*, pages 3286–3290, 2017. doi: 10.23919/EuCAP.2017.7928583.
- [10] S. Boyd. Multitone Signals with Low Crest Factor. *IEEE Transactions on Circuits and Systems*, 33(10):1018–1022, 1986. doi: 10.1109/TCS.1986.1085837.
- [11] Christina Chaccour, Mehdi Naderi Soorki, Walid Saad, Mehdi Bennis, Petar Popovski, and Mérouane Debbah. Seven Defining Features of Terahertz (THz) Wireless Systems: A Fellowship of Communication and Sensing. *IEEE Communications Surveys & Tutorials*, 24(2):967–993, 2022. doi: 10.1109/COMST.2022.3143454.
- [12] Qi Chen, Alexander Wyglinski, and Gary Minden. Frequency Agile Interference-Aware Channel Sounding for Dynamic Spectrum Access Networks. In *IEEE GLOBECOM 2007 - IEEE Global Telecommunications Conference*, pages 3144–3148, 2007. doi: 10.1109/GLOCOM.2007.595.

- [13] Yi Chen, Yuanbo Li, Chong Han, Ziming Yu, and Guangjian Wang. Channel Measurement and Ray-Tracing-Statistical Hybrid Modeling for Low-Terahertz Indoor Communications. *IEEE Transactions on Wireless Communications*, 20(12):8163–8176, 2021. doi: 10.1109/TWC.2021.3090781.
- [14] Chia-Lin Cheng, Seunghwan Kim, and Alenka Zajić. Comparison of path loss models for indoor 30 GHz, 140 GHz, and 300 GHz channels. In *2017 11th European Conference on Antennas and Propagation (EUCAP)*, pages 716–720, 2017. doi: 10.23919/EuCAP.2017.7928124.
- [15] Aditya Chopra, Andrew Thornburg, Ojas Kanhere, Saeed S. Ghassemzadeh, Milap Majmundar, and Theodore S. Rappaport. A Real-Time Millimeter Wave V2V Channel Sounder. In *2022 IEEE Wireless Communications and Networking Conference (WCNC)*, pages 2607–2612, 2022. doi: 10.1109/WCNC51071.2022.9772001.
- [16] D. Cox. Delay Doppler characteristics of multipath propagation at 910 MHz in a suburban mobile radio environment. *IEEE Transactions on Antennas and Propagation*, 20(5):625–635, 1972. doi: 10.1109/TAP.1972.1140277.
- [17] Linglong Dai, Zhen Gao, and Zhaocheng Wang. Joint channel estimation and feedback with low overhead for FDD massive MIMO systems. In *2015 IEEE/CIC International Conference on Communications in China (ICCC)*, pages 1–6, 2015. doi: 10.1109/ICCChina.2015.7448660.
- [18] Ravilla Dilli. Analysis of 5G Wireless Systems in FR1 and FR2 Frequency Bands. In *2020 2nd International Conference on Innovative Mechanisms for Industry Applications (ICIMIA)*, pages 767–772, 2020. doi: 10.1109/ICIMIA48430.2020.9074973.
- [19] *D-Band Low Noise Amplifier*. Eravant, 2020. URL <https://sftp.eravant.com/content/datasheets/SBL-1141743065-0606-E1.pdf>. Datasheet.

- [20] *D-Band Power Amplifier*. Eravant, 2020. URL <https://sftp.eravant.com/content/datasheets/SBP-1141543010-0606-E1.pdf>. Datasheet.
- [21] *D-Band, X12 Active Multiplier*. Eravant, 2022. URL <https://sftp.eravant.com/content/datasheets/SFA-1141741202-06SF-E1.pdf>. Datasheet.
- [22] *Frequency Synthesizer Module, Low Phase Noise*. Eravant, 2022. URL <https://sftp.eravant.com/content/datasheets/SOT-02220313200-SF-B6.pdf>. Datasheet.
- [23] *WR-06 Dual Polarized Scalar Feed Horn Antenna*. Eravant, 2023. URL <https://sftp.eravant.com/content/datasheets/SAF-1141741525-082-S1-065-DP.pdf>. Datasheet.
- [24] Ericsson. Ericsson Mobility Report, November 2023. <https://www.ericsson.com/4ae12c/assets/local/reports-papers/mobility-report/documents/2023/ericsson-mobility-report-november-2023.pdf>. [Online].
- [25] ETSI - European Telecommunications Standards Institute. 5G; NR; Base Station (BS) radio transmission and reception (3GPP TS 38.104 version 16.4.0 Release 16). Technical Report ETSI TS 138 104, ETSI, March 2022. URL https://www.etsi.org/deliver/etsi_ts/138100_138199/138104/16.04.00_60/ts_138104v160400p.pdf. Accessed: 2024-11-15.
- [26] Ettus Research. USRP B200/B210 Bus Series, 2019. [Online]. Available: https://www.ettus.com/wp-content/uploads/2019/01/b200-b210_spec_sheet.pdf.
- [27] Niels Hendrik Fliedner, Dimitri Block, and Uwe Meier. A Software-Defined Channel Sounder for Industrial Environments with Fast Time Variance. In *2018 15th International Symposium on Wireless Communication Systems (ISWCS)*, pages 1–6, 2018. doi: 10.1109/ISWCS.2018.8491207.

- [28] Samantha Frietchen, Daniel J. Jakubisin, and Alan J. Michaels. Semi-Automation of Wideband Channel Sounding Transmitter. In *2024 IEEE International Symposium on Dynamic Spectrum Access Networks (DySPAN)*, pages 145–150, 2024. doi: 10.1109/DySPAN60163.2024.10632753.
- [29] Samantha Frietchen, Michael J. Fletcher, Daniel J. Jakubisin, and Alan J. Michaels. D-Band Path Loss Measurements and Frequency Stability Characterization. In *2025 the 5th European Conference on Communication Systems (ECCS 2025)*, 2025. [Accepted].
- [30] Samantha Frietchen, Daniel J. Jakubisin, and Alan J. Michaels. Channel Sounding Waveform Comparison using Software Defined Radios. In *2025 the 5th European Conference on Communication Systems (ECCS 2025)*, 2025. [Accepted].
- [31] Anirban Ghosh and Minseok Kim. THz Channel Sounding and Modeling Techniques: An Overview. *IEEE Access*, 11:17823–17856, 2023. doi: 10.1109/ACCESS.2023.3246161.
- [32] Giovanni Giambene, MD Saifur Rahman, and Alexey Vinel. Analysis of V2V Sidelink Communications for Platoon Applications. In *ICC 2020 - 2020 IEEE International Conference on Communications (ICC)*, pages 1–6, 2020. doi: 10.1109/ICC40277.2020.9148968.
- [33] Ke Guan, Bile Peng, Danping He, Johannes M. Eckhardt, Haofan Yi, Sebastian Rey, Bo Ai, Zhangdui Zhong, and Thomas Kürner. Channel Sounding and Ray Tracing for Intrawagon Scenario at mmWave and Sub-mmWave Bands. *IEEE Transactions on Antennas and Propagation*, 69(2):1007–1019, 2021. doi: 10.1109/TAP.2020.3016399.
- [34] Chong Han, Yiqin Wang, Yuanbo Li, Yi Chen, Naveed A. Abbasi, Thomas Kürner, and Andreas F. Molisch. Terahertz Wireless Channels: A Holistic Survey on Measurement,

- Modeling, and Analysis. *IEEE Communications Surveys & Tutorials*, 24(3):1670–1707, 2022. doi: 10.1109/COMST.2022.3182539.
- [35] Chong Han, Weijun Gao, Nan Yang, and Josep M. Jornet. Molecular Absorption Effect: A Double-Edged Sword of Terahertz Communications. *IEEE Wireless Communications*, 30(4):140–146, 2023. doi: 10.1109/MWC.016.2100704.
- [36] Attila Hilt. Feasibility of D-band Fixed Radio Links for 5G and Beyond Access Networks. In *2024 34th International Conference Radioelektronika (RADIOELEKTRONIKA)*, pages 1–6, 2024. doi: 10.1109/RADIOELEKTRONIKA61599.2024.10524063.
- [37] Nozhan Hosseini and David W. Matolak. Wide band channel characterization for low altitude unmanned aerial system communication using software defined radios. In *2018 Integrated Communications, Navigation, Surveillance Conference (ICNS)*, pages 2C2–1–2C2–9, 2018. doi: 10.1109/ICNSURV.2018.8384840.
- [38] Md Biplob Hossen, Mostafa Zaman Chowdhury, and Mohammad Ehatasham Shawon. Spreading Loss Model for Channel Characterization of Future 6G Terahertz Communication Networks. In *2021 3rd International Conference on Electrical & Electronic Engineering (ICEEE)*, pages 25–28, 2021. doi: 10.1109/ICEEE54059.2021.9718778.
- [39] Shihao Ju, Syed Hashim Ali Shah, Muhammad Affan Javed, Jun Li, Girish Palteru, Jyotish Robin, Yunchou Xing, Ojas Kanhere, and Theodore S. Rappaport. Scattering Mechanisms and Modeling for Terahertz Wireless Communications. In *ICC 2019 - 2019 IEEE International Conference on Communications (ICC)*, pages 1–7, 2019. doi: 10.1109/ICC.2019.8761205.
- [40] Sung Yun Jun, Derek Caudill, Jack Chuang, Peter B. Papazian, Anuraag Bodi, Camillo Gentile, Jelena Senic, and Nada Golmie. Penetration Loss at 60 GHz for Indoor-to-Indoor and Outdoor-to-Indoor Mobile Scenarios. In *2020 14th European Conference on*

- Antennas and Propagation (EuCAP)*, pages 1–5, 2020. doi: 10.23919/EuCAP48036.2020.9135581.
- [41] Edward Kassem, Roman Marsalek, and Jiri Blumenstein. Frequency Domain Zadoff-Chu Sounding Technique for USRPs. In *2018 25th International Conference on Telecommunications (ICT)*, pages 302–306, 2018. doi: 10.1109/ICT.2018.8464940.
- [42] Wilhelm Keusgen and Taro Eichler. Probing the Time-Evolution of the Sub-THz Radio Channel at 160 GHz for Communication and Sensing. In *2024 IEEE 99th Vehicular Technology Conference (VTC2024-Spring)*, pages 01–07, 2024. doi: 10.1109/VTC2024-Spring62846.2024.10683181.
- [43] Chung-Sup Kim, Hyuk-Je Kim, Sung-Woong Choi, Kwan-Woong Ryu, and Jun-Seok Kim. Propagation characteristics of various highway V2V environment at 5.9GHz Band. In *2022 13th International Conference on Information and Communication Technology Convergence (ICTC)*, pages 2026–2030, 2022. doi: 10.1109/ICTC55196.2022.9952763.
- [44] Joonas Kokkonen, Janne Lehtomäki, and Markku Juntti. Measurements on Penetration Loss in Terahertz Band. In *2016 10th European Conference on Antennas and Propagation (EuCAP)*, pages 1–5, 2016. doi: 10.1109/EuCAP.2016.7481176.
- [45] G. G. Kumar, S. K. Sahoo, and P. K. Meher. 50 Years of FFT Algorithms and Applications. *Circuits, Systems, and Signal Processing*, pages 5665–5698, 2019. doi: 10.1007/s00034-019-01136-8.
- [46] L-com. 1.2 GHz 8 dBi Flat Patch Antenna. <https://www.l-com.com/wireless-antenna-12-ghz-8-dbi-flat-patch-antenna-sma-male-connector>.
- [47] Byeong Gi Lee, Daeyoung Park, and Hanbyul Seo. *Characteristics of Wireless Channels*, pages 9–39. 2009. doi: 10.1002/9780470823583.ch2.

- [48] Gang Li, Jin Teng, Fan Yang, Adam C. Champion, Dong Xuan, Hong Luan, and Yuan F. Zheng. EV-sounding: A visual assisted electronic channel sounding system. In *IEEE INFOCOM 2014 - IEEE Conference on Computer Communications*, pages 1483–1491, 2014. doi: 10.1109/INFOCOM.2014.6848083.
- [49] Jing Li, Peize Zhang, Chen Yu, Haiming Wang, and Wei Hong. High-Efficiency Wide-band Millimeter-Wave Channel Sounder System. In *2019 13th European Conference on Antennas and Propagation (EuCAP)*, pages 1–5, 2019.
- [50] Lu Li, Aduwati Sali, and Sangin Qahtan Wali. Atmospheric Attenuation at mmWave Below 57GHz Based on Measurement in Tropical Region. In *2023 IEEE 16th Malaysia International Conference on Communication (MICC)*, pages 65–69, 2023. doi: 10.1109/MICC59384.2023.10419466.
- [51] R. Li. Network 2030: Market drivers and prospects. In *Proc. 1st Int. Telecommun. Union (ITU-T) Workshop Netw.*, pages 1–21, Oct. 2018.
- [52] Mir Lodro, Gabriele Gradoni, Ana Vukovic, Dave Thomas, and Steve Greedy. Time-Domain Wireless Channel Sounding Using Software Defined Radio. In *2020 3rd International Conference on Computing, Mathematics and Engineering Technologies (iCoMET)*, pages 1–5, 2020. doi: 10.1109/iCoMET48670.2020.9073860.
- [53] Yejian Lyu, Pekka Kyösti, and Wei Fan. Sub-terahertz channel sounder: Review and future challenges. *China Communications*, 20(6):26–48, 2023. doi: 10.23919/JCC.fa.2021-0450.202306.
- [54] Jianjun Ma, Lucas Vorrius, Francis amd Lamb, Lothar Moeller, and John F. Federici. Comparison of Experimental and Theoretical Determined Terahertz Attenuation in Controlled Rain. *J. Infr., Millim., THz Waves*, 36(12):1195–1202, 2015. doi: 10.1007/s10762-015-0200-6.

- [55] George R. MacCartney and Theodore S. Rappaport. A Flexible Millimeter-Wave Channel Sounder With Absolute Timing. *IEEE Journal on Selected Areas in Communications*, 35(6):1402–1418, 2017. doi: 10.1109/JSAC.2017.2687838.
- [56] Andreas F. Molisch. Channel Models. In *Wireless Communications*, pages 125–143. IEEE, 2011. doi: 10.1002/9781119992806.ch7.
- [57] Braeden P. Muller, Lauren J. Wong, William H. Clark, and Alan J. Michaels. A Real-World Dataset Generator for Specific Emitter Identification. *IEEE Access*, 11:110023–110038, 2023. doi: 10.1109/ACCESS.2023.3322105.
- [58] Berthold Panzner, Taylan Şahin, and Prajwal Keshavamurthy. Coexistence of 5G Sidelink Communication and 5G Sidelink Positioning. In *2022 International Symposium ELMAR*, pages 77–80, 2022. doi: 10.1109/ELMAR55880.2022.9899798.
- [59] Radoslaw Piesiewicz, Christian Jansen, Daniel Mittleman, Thomas Kleine-Ostmann, Martin Koch, and Thomas Kurner. Scattering Analysis for the Modeling of THz Communication Systems. *IEEE Transactions on Antennas and Propagation*, 55(11):3002–3009, 2007. doi: 10.1109/TAP.2007.908559.
- [60] Ryan J. Pirkl and Gregory D. Durgin. Optimal Sliding Correlator Channel Sounder Design. *IEEE Transactions on Wireless Communications*, 7(9):3488–3497, 2008. doi: 10.1109/TWC.2008.070278.
- [61] T. S. Rappaport. *Wireless Communications: Principles and Practice*. Prentice-Hall, New Jersey, 2nd edition, 2002.
- [62] Theodore S. Rappaport, Shu Sun, Rimma Mayzus, Hang Zhao, Yaniv Azar, Kevin Wang, George N. Wong, Jocelyn K. Schulz, Mathew Samimi, and Felix Gutierrez. Mil-

- limeter Wave Mobile Communications for 5G Cellular: It Will Work! *IEEE Access*, 1: 335–349, 2013. doi: 10.1109/ACCESS.2013.2260813.
- [63] S. Salous, P. Pantzaris, and P. Green. FMCW Waveforms for UHF/SHF Wideband Channel Sounders. In *IEE Colloquium on High Bit Rate UHF/SHF Channel Sounders - Technology and Measurement*, pages 2/1–2/5, 1993.
- [64] Saeed Salous. *Radio Propagation Measurement and Channel Modeling*. John Wiley & Sons, Chichester, UK, 2013.
- [65] Yasser Samayoa, Markus Kock, Holger Blume, and Jörn Ostermann. Low-Cost Channel Sounder Design Based on Software-Defined Radio and OFDM. In *2018 IEEE 88th Vehicular Technology Conference (VTC-Fall)*, pages 1–5, 2018. doi: 10.1109/VTCFall.2018.8690695.
- [66] M. Sandra, C. Nelson, and A. J. Johansson. Ultrawideband USRP-Based Channel Sounding Utilizing the RFNoC Framework. In *2022 IEEE Conference on Antenna Measurements and Applications (CAMA)*, pages 1–3, Guangzhou, China, 2022. doi: 10.1109/CAMA56352.2022.10002476.
- [67] Hadi Sardeddeen, Mohamed-Slim Alouini, and Tareq Y. Al-Naffouri. An Overview of Signal Processing Techniques for Terahertz Communications. *Proceedings of the IEEE*, 109(10):1628–1665, 2021. doi: 10.1109/JPROC.2021.3100811.
- [68] Alper Schultze, Mathis Schmieder, Ramez Askar, Michael Peter, Wilhelm Keusgen, and Taro Eichler. Comparison of Sub-THz Radio Channel Characteristics at 158 GHz and 300 GHz in a Shopping Mall Scenario. In *2024 18th European Conference on Antennas and Propagation (EuCAP)*, pages 1–5, 2024. doi: 10.23919/EuCAP60739.2024.10501599.

- [69] Kibeom Seong, Mehdi Mohseni, and John M. Cioffi. Optimal Resource Allocation for OFDMA Downlink Systems. In *2006 IEEE International Symposium on Information Theory*, pages 1394–1398, 2006. doi: 10.1109/ISIT.2006.262075.
- [70] Dipankar Shakya, Ting Wu, Michael E. Knox, and Theodore S. Rappaport. A Wideband Sliding Correlation Channel Sounder in 65 nm CMOS: Evaluation Board Performance. *IEEE Transactions on Circuits and Systems II: Express Briefs*, 68(9):3043–3047, 2021. doi: 10.1109/TCSII.2021.3087032.
- [71] M. M. Silva et al. Evaluation of OFDM Channel Sounding Techniques with Three Modulation Sequences. *Journal of Microwaves Optoelectronics and Electromagnetic Applications*, 18(4):505–529, November 2019. doi: 10.1590/2179-10742019v18i41704.
- [72] R. M. L. Silva et al. Comparison between OFDM and STDCC Mobile Channel Sounders at 3.5 GHz. *Journal of Microwaves, Optoelectronics and Electromagnetic Applications*, 12:1–14, June 2013. doi: 10.1590/S2179-10742013000100001.
- [73] M.R. Souryal and R.L. Pickholtz. Adaptive modulation with imperfect channel information in OFDM. In *ICC 2001. IEEE International Conference on Communications. Conference Record (Cat. No.01CH37240)*, volume 6, pages 1861–1865 vol.6, 2001. doi: 10.1109/ICC.2001.937113.
- [74] Daniel Stanko, Gerd Sommerkorn, Alexander Ihlow, and Giovanni Del Galdo. Enable SDRs for Real-Time MIMO Channel Sounding featuring Parallel Coherent Rx Channels. In *2022 IEEE 95th Vehicular Technology Conference: (VTC2022-Spring)*, pages 1–5, 2022. doi: 10.1109/VTC2022-Spring54318.2022.9860841.
- [75] Richard Tanski, D’Andre Seymour, Bryan Heredia, Christopher Slezak, Vasanthan Raghavan, Vito Salluce, Ozge Koymen, Amit Mathur, and Arumugam Kannan. Sub-

- THz Wireless Channel Field Measurements: A Study at 140 GHz. In *2022 IEEE Globecom Workshops (GC Wkshps)*, pages 1790–1795, 2022. doi: 10.1109/GCWkshps56602.2022.10008496.
- [76] Harsh Tataria, Mansoor Shafi, Andreas F. Molisch, Mischa Dohler, Henrik Sjöland, and Fredrik Tufvesson. 6G Wireless Systems: Vision, Requirements, Challenges, Insights, and Opportunities. *Proceedings of the IEEE*, 109(7):1166–1199, 2021. doi: 10.1109/JPROC.2021.3061701.
- [77] Vitrek. Ultra-Portable RF Signal Recorders. <https://vitrek.com/gage/systems/ultra-portable-rf-signal-recorders/>.
- [78] *Ultra-Portable RF Signal Recorders*. Vitrek. URL <https://vitrek.com/gage/systems/ultra-portable-rf-signal-recorders/>. Datasheet.
- [79] Dereje Assefa Wassie, Ignacio Rodriguez, Gilberto Berardinelli, Fernando M. L. Tavares, Troels B. Sørensen, Thomas L. Hansen, and Preben Mogensen. An Agile Multi-Node Multi-Antenna Wireless Channel Sounding System. *IEEE Access*, 7:17503–17516, 2019. doi: 10.1109/ACCESS.2019.2895412.
- [80] Robert White and David G Michelson. Application of cognitive radio principles to wireless channel sounding. In *2014 16th International Symposium on Antenna Technology and Applied Electromagnetics (ANTEM)*, pages 1–2, 2014. doi: 10.1109/ANTEM.2014.6887672.
- [81] Ian C. Wong and Brian L. Evans. Optimal Downlink OFDMA Resource Allocation with Linear Complexity to Maximize Ergodic Rates. *IEEE Transactions on Wireless Communications*, 7(3):962–971, 2008. doi: 10.1109/TWC.2008.4472014.
- [82] Yunchou Xing and Theodore S. Rappaport. Propagation Measurements and Path Loss

- Models for sub-THz in Urban Microcells. In *ICC 2021 - IEEE International Conference on Communications*, pages 1–6, 2021. doi: 10.1109/ICC42927.2021.9500385.
- [83] Ziming Yu, Yi Chen, Guangjian Wang, Weijun Gao, and Chong Han. Wideband Channel Measurements and Temporal-Spatial Analysis for Terahertz Indoor Communications. In *2020 IEEE International Conference on Communications Workshops (ICC Workshops)*, pages 1–6, 2020. doi: 10.1109/ICCWorkshops49005.2020.9145314.
- [84] Yamen Zantah, Mai Alissa, Theo Kreul, and Thomas Kaiser. Ultra-wideband Multipath Channel Characterization at 300 GHz. In *WSA 2020; 24th International ITG Workshop on Smart Antennas*, pages 1–5, 2020.
- [85] T. Zwick, T.J. Beukema, and Haewoon Nam. Wideband Channel Sounder with Measurements and Model for the 60 GHz Indoor Radio Channel. *IEEE Transactions on Vehicular Technology*, 54(4):1266–1277, 2005. doi: 10.1109/TVT.2005.851354.